Russian Chemical Reviews **75** (1) 57 – 76 (2006) © 2006 Russian Academy of Sciences and Turpion Ltd

DOI 10.1070/RC2006v075n01ABEH001184

Crystalline water ices

E A Zheligovskaya, G G Malenkov

Contents

I.	Introduction	57
II.	General remarks	57
III.	Recent data on the structures and proton ordering of crystalline water ices. Phase transitions between crystalline ices	58
IV.	Inelastic neutron scattering spectroscopy of water ices	69
V.	Computer simulations of crystalline ices	70
VI.	Occurrence of high-pressure ices in nature	73
VII.	Appendix	73

Abstract. Recent publications on the structures of crystalline water ices are surveyed. Interconversions of crystalline and amorphous ices are considered. Some hypotheses concerning the occurrence of high-pressure ices in nature are outlined. The bibliography includes 149 references.

I. Introduction

The properties of crystalline and amorphous water ices have been attracting steady interest of researchers for several reasons. First, water plays the most important role in biological processes and thus the knowledge of typical structures formed by water molecules may help elucidating the structures of water bound to proteins or other biological macromolecules. Second, water is one of the most abundant substances in the universe and thus investigations into potential states that can be adopted by water in the interstellar space or other orbs are of great interest. Third, studies of water are of general theoretical importance since they give insights into the common regularities of structure and polymorphism of various substances featuring tetrahedral coordination of molecules or atoms, the reasons underlying the existence of several amorphous forms of a substance and the regularities of phase transitions between them, the nature of pressure-induced amorphisation of crystals and solid-state crystallisation from an amorphous state and many other issues.

The present review concerns structural studies of crystalline water ices. We survey the data on the structures of crystalline forms of ice and transitions between them published over the last 10 – 15 years and consider related topics, in particular, amorphisation of crystalline ices and their crystallisation from amorphous phases. Some earlier papers are cited where appropriate. A comprehensive review of studies published before 1974 can be found elsewhere.[1]

E A Zheligovskaya, G G Malenkov A N Frumkin Institute of Physical Chemistry and Electrochemistry, Russian Academy of Sciences, Leninsky prosp. 31, 119991 Moscow, Russian Federation, Fax (7-495) 952 53 08, tel. (7-495) 955 44 21, e-mail: lmm@phyche.ac.ru

Received 24 May 2005
Uspekhi Khimii **75** (1) 64 – 85 (2006); translated by Ya V Zubavichus

II. General remarks

At present, thirteen reliably established crystalline modifications of water ices are known (Fig. 1 and Appendix, numbering of the crystalline phases reflects the order of their discovery). These

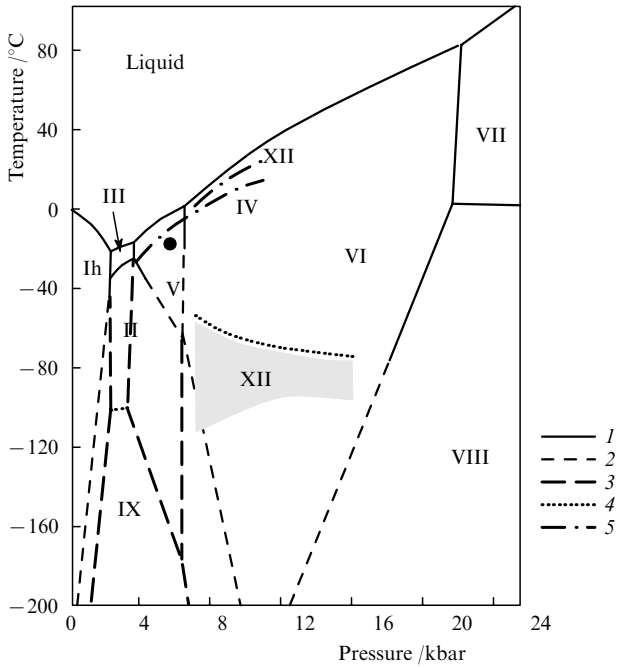


Figure 1. The low-temperature part of the water phase diagram at pressures up to 2.5 GPa.
(*1*) The experimentally determined lines of stable phase equilibria, (*2*) the calculated and extrapolated lines of stable phase equilibria, (*3*) the experimentally determined and calculated lines of metastable phase equilibria, (*4*) the experimental curve [2] for the maximum rate of the transformation of ice III into ice IX within the region of stability of ice II and the curve for the transformation [3] of metastable ice XII into stable ice VI, (*5*) the experimentally determined melting curves of metastable ices IV [4] and XII,[5] the bold dot indicates the region where ice XII was prepared for the first time [6] by crystallisation from liquid, the second area of the existence [3] of ice XII prepared by crystallisation of high-density amorphous ice (HDA, see Section III.6) is marked grey.

forms of ice can be reproducibly prepared using *ad hoc* techniques, they have been thoroughly characterised by spectroscopy and their crystal structures have been determined using X-ray or neutron diffraction. Some of the known crystalline modifications of ice are characterised by specific regions of the stability in the water phase diagram, whereas others (*viz*., Ic, IV, IX and XII) occur exclusively as metastable states. It is of note that the recently discovered metastable ice XII can occur in two separate regions of the phase diagram.

In the structures of all known crystalline ices, each water molecule forms four hydrogen bonds directed towards vertices of an ideal or slightly distorted tetrahedron with neighbouring molecules. In all cases except for ice X, the H_2O molecules retain their integrity and act as donors of hydrogen atoms for two out of the four hydrogen bonds and as aceptors for two other bonds.

The normal-pressure crystalline phases (Ih, Ic and XI) are characterised by nearly ideal tetrahedral closest environment of water molecules. Meanwhile, in high-pressure phases (II, III, IX, V, IV, XII andVI), the oxygen atoms of neighbouring molecules occupy vertices of a distorted tetrahedron. The framework of hydrogen bonds becomes self-entangled starting from a pressure of ~ 0.5 GPa (ices IV and V), which means that it represents an integral network where at least some elementary H-bond cycles appear hooked to each other. At higher pressure, phases composed of two independent interpenetrating frameworks of hydrogen bonds are formed (crystalline ices VI, VII and VIII). Unlike self-entangled frameworks, these ices contain two interpenetrating non-linked H-bond networks. At a pressure of the order of 2 GPa or higher, nearly ideal tetrahedral coordination of water molecules is recovered (ices VII and VIII). Finally, at even higher pressures, the oxygen sublattice of ices VII and VIII is preserved but the hydrogen atoms are shifted towards the centres of the $O-H\cdots O$ bonds. Consequently, starting from ~ 50 GPa, the hydrogen atoms become evenly shared between the two neighbouring oxygen atoms and the molecular structure is transformed in a framework structure in crystalline ice X. Such a structure is maintained at pressures of up to 200 GPa, which is the highest value explored to date.

Protons in the crystalline water ices occupy the respective positions near the oxygen atoms in a regular or random way. In proton-ordered ices, the two neighbouring molecules involved in donor-type H-bonding and those two involved in acceptor-type H-bonding are defined unambiguously (in other words, the orientation of water molecules with respect to their closest neighbours is known). Two of the four possible positions of the H atoms near an O atom have occupancies close to unity (they are equal to unity in the case of complete ordering), whereas two other positions have occupancies close to zero (they are equal to zero in the case of complete ordering). In the case of proton-disordered ices, each of the four hydrogen bonds formed by a water molecule can serve simultaneously as both the donor and the acceptor such that four possible hydrogen positions around the respective oxygen atom have equal occupancies of 0.5. In a sense, water molecules in these proton-disordered ice modifications adopt arbitrary orientations with respect to their closest neighbours in the crystal structure. The situation with the occupancies of some hydrogen positions significantly differing from 0, 0.5 or 1 is referred to as a partial (dis)order. Ices II and VIII are completely proton-ordered; ice IX is partially proton-ordered; the proton-ordered ice XI has been obtained only as nanocrystallites embedded into a matrix of ice Ih, thus the extent of its proton-ordering cannot be reliably analysed; other ices are completely or partially proton-disordered.

Since water molecules preserve their integrity and form exactly two donor and two acceptor H-bonds with neighbouring water molecules in all but ice X water ices, the disordering of proton positions in the crystal structures of proton-disordered ices obeys the so-called Bernal–Fowler rules:[7] (i) exactly two H atoms are located around each oxygen atom at a distance of the covalent bond; (ii) each hydrogen bond accomodates exactly one hydrogen atom. A violation of the first rule gives rise to ionic defects (*i.e*., the occurrence of H_3O^+ or OH^- ions instead of H_2O molecules); a violation of the second rule results in the Bjerrum defects (*i.e*., the coexistence of two hydrogen atoms or a hydrogen vacancy along a hydrogen bond, also referred to as D- and L-defects, respectively).

Among the known ice polymorphs, several pairs of crystalline modifications having identical oxygen sublattices but differing from each other in the extent of the proton ordering can be distinguished. These include proton-disordered ices Ih, III and VII with their proton-ordered counterparts, ices XI, IX and VIII, respectively. Since orientations of water molecules relative to their closest neighbours within these pairs are different, these phases have different dynamical characteristics and, as a consequence, vibrational spectra. These differences are manifested in the IR, Raman and inelastic neutron scattering (INS) spectra.

Several water ices have close structural analogues among other crystalline substances built up of tetrahedrally coordinated atoms. In particular, lonsdalite (hexagonal diamond modification), wurtzite (ZnS) and high-temperature tridymite (SiO_2) are isostructural to ice Ih; diamond, silicon, germanium, grey tin, high-temperature cristobalite (SiO_2) and sphalerite (ZnS) are isostructural to ice Ic; high-pressure germanium and keatite (SiO_2) are isostructural to ices III and IX; the aluminosilicate framework of eddingtonite $Ba(Al_2Si_3O_{10})$ is isostructural to one of two identical independent interpenetrating frameworks of ice VI. Note that Zn and S atoms in the frameworks of wurtzite and sphalerite alternate in positions occupied by the oxygen atoms in the corresponding ices Ih and Ic. In SiO_2 polymorphs isostructural to crystalline ices, H-bonded oxygen sublattice is replaced by similar frameworks of silicon atoms linked by covalent $Si-O-Si$ bonds.

The discovery of a new crystalline phase of water, namely, the metastable ice XII, is probably the most outstanding recent achievement in the studies of crystalline water ices. The crystal structure of this phase, which has no analogues among substances with the tetrahedral coordination of atoms, has been determined; two regions of its stability in the water phase diagram have been established and the parallel crystallisation of ices IV and XII from amorphous high-density ice has been observed. In addition, the presence and extent of proton ordering in various water ices, the boundaries of their stability and metastability in the phase diagram as well as their thermodynamical parameters were specified in studies of the last decade. Phase transitions between ice polymorphs have been investigated. IR, Raman and INS spectra have been collected for all known ice phases. In parallel, vibrational spectra of various ices have been calculated theoretically using the lattice dynamics method. Finally, the molecular dynamics has been applied to simulate the existing and hypothetical crystalline water ices. The results of these studies are considered below.

III. Recent data on the structures and proton ordering of crystalline water ices. Phase transitions between crystalline ices

1. Ices Ih, Ic and XI

Hexagonal ice Ih, its proton-ordered low-temperature analogue, ice XI, and metastable cubic ice Ic constitute the group of normal-pressure (1 bar) crystalline water ices. Among these modifications, ice Ih, which is formed upon freezing of water at a pressure from 0 to ~ 0.2 GPa, is studied the best. Metastable ice Ic with the structure relating to that of ice Ih in the same way as the structure of diamond relates to that of lonsdalite can be prepared by deposition of water vapour on a cold ($163 < T < 183$ K) metal support,[8] rapid cooling of emulsions composed of water microdroplets down to $150 < T < 190$ K (at a cooling rate of 10^6-10^7 K s^{-1}),[9] freezing of water in capillaries [10,11] (see below in this Section) and heating of quenched high-pressure crystalline [12–18] (see Section III.8) or amorphous [19–21] (see Sec-

tion III.6) water ices at a pressure of 1 bar. Irrespective of the preparation method, annealing of ice Ic initiates its irreversible conversion into ice Ih. The temperature of this transition depends on the heating rate and prehistory of the sample and lies in the range from 140 to 230 K.

The unit cell parameters a and c of ices Ih(H_2O) and Ih(D_2O) were measured [22] by powder X-ray diffraction using synchrotron radiation in a wide temperature range from 10 to 265 K at a constant pressure of 100 Torr. The unit cell parameters of ice Ih(D_2O) were slightly larger than those of ice Ih(H_2O) in the whole temperature range. The a/c ratio was virtually independent of temperature indicating that the thermal expansion of ice Ih can be considered isotropic. The linear thermal expansion coefficients (α) of both ices Ih(H_2O) and Ih(D_2O) are negative below 75 K, which means that these phases expand upon cooling. Such a behaviour is also typical of other substances with the tetrahedral coordination of atoms.[22] Below 100 K, the coefficients α_{H_2O} and α_{D_2O} are the same but the increase in α_{D_2O} above 100 K occurs faster than that of α_{H_2O}.

The linear thermal expansion coefficients of ices Ih and Ic were also calculated theoretically using the TIP4P intermolecular interaction potential [23] with averaging over a large ensemble of possible proton configurations.[24] These calculations confirmed that the coefficients α for both ices Ic and Ih should become negative at low temperature. Similar calculations [25] for ices Ic and VII based on the Carravetta–Clementi potential [26] showed that $\alpha < 0$ for ice Ic at low temperature, whereas the linear thermal expansion coefficient is always positive for ice VII, which represents two independent interposed frameworks of ice Ic.

It is known that ice Ih is proton-disordered and this positional proton disorder persists upon cooling down to 0 K.[7] Meanwhile, according to the third law of thermodynamics, only one thermodynamically stable structure with a specific arrangement of protons should exist at 0 K at any given pressure. Such a transition to the equilibrium structure cannot be realised for chemically pure water due to the vanishingly low orientational mobility of H_2O molecules in the crystal structure of ice Ih. Introduction of a minute amount of hydroxide anions into water results in the formation of defects distorting the framework of H-bonds, which facilitates the phase transition of the crystalline ice Ih to the proton-ordered state. Such a transition has indeed been observed at 72 K in calorimetric experiments and measurements of dielectric properties.[27] This new phase representing a proton-ordered low-temperature analogue of ice Ih was entitled [27] ice XI, since phases II–X had already been known to that moment.

The crystal structure of heavy ice XI(D_2O) doped with KOD was investigated using powder neutron diffraction.[28] High-resolution powder neutron diffraction was also applied to elucidate the structure of normal ice XI(H_2O) doped with KOH.[29] The results obtained were consistent with the orthorhombic structure corresponding to the space group $Cmc2_1$ with the protons ordered into a ferroelectric phase. It has to be mentioned that the same structure was predicted earlier based on a theoretical analysis.[28,29] Nevertheless, the fraction of the ordered phase as revealed in the neutron diffraction studies [28,29] was low, and the major structural information in these measurements related to disordered ice Ih. Thus, the cited studies left open the question on the structure of ice XI. Furthermore, a series of theoretical studies of the ordered structures with a framework of water molecules based on ice Ih [30–32] claimed a structure corresponding to the space group $Pna2_1$ with the antiferroelectric ordering of protons and eight water molecules per unit cell to be the most stable. Therefore, the results of neutron diffraction studies [28,29] were contested and thus the character of the proton ordering in the crystal structure of ice XI remained a subject of debate for a long time.

Recently, Jackson and Whitworth,[33,34] using a newly developed method of temperature-stimulated depolarisation, which is based on the generation of an electric current pulse in the transition of a polarised ice into the disordered state upon heating, have shown that the proton ordering in the structure of ice XI corresponds to a ferroelectric with a non-zero dipole moment along the c axis and the zero dipole moment in the ab plane. Further investigations into the structure of ice XI(D_2O) using high-resolution powder neutron diffraction [35] and of ice XI(H_2O) using neutron diffraction on a quasi-single crystal [36] obtained from ice Ih that underwent the phase transition Ih → XI and contained about 37% of ice XI, also confirmed the orthorhombic structure of ice XI with the space group $Cmc2_1$. Neighbouring hexagonal layers in this structure are somewhat shifted with respect to each other, which probably plays the decisive role in the stabilisation of the ferroelectric structure. It has been shown that the diffraction pattern of ice XI manifests the (131) reflection, which is forbidden for ice Ih (in the corresponding orthorhombic setting).

The formation of ice XI from a single crystal of Ih(D_2O) grown from a 0.1 M KOD solution kept for 520 h at 62 K and for 88 h at 68 K was also studied by neutron diffraction.[37] [The temperature of transition to ice XI for KOD-doped Ih(D_2O) was 76 K.] The extent of conversion was monitored by the intensity of the (131) reflection, which first increased and then reached a plateau. The degree of conversion of ice as a function of time and the ultimate degree of conversion at $t \to \infty$ (*i.e.*, 38.2% at 62 K and 47.9% at 68 K for the 0.1 M KOD solution in D_2O used to grow the single crystal of Ih) were determined. The results obtained can be explained by the emergence of numerous nucleation sites of ice XI inside the single crystal of Ih (most probably, around the OD^- ions) followed by growth of ordered domains of ice XI around these sites. The characteristic size of ice XI domains depending on temperature, duration of storage and KOD concentration in the solution did not exceed [37] 60 Å under the conditions used. However, it remains unclear, why the transition stopped very far from the complete conversion of the samples into ice XI with randomly oriented contacting domains. It is of note that storage of the KOD-doped ice Ih for 40 h at 51 K yielded no detectable amounts of ice XI.

The crystal structure of ice Ih has two different mutual orientations of H-bonded water molecules lying in adjacent hexagonal layers (Fig. 2 *a*,*b*) and two different orientations of H-bonded water molecules within the same hexagonal layer (Fig. 2 *c*,*d*). Due to the electrostatic repulsion, the energy of the molecular pairs depicted in Figs 2 *b* and 2 *d* is higher than that of the pairs depicted in Figs 2 *a* and 2 *c*, respectively. Within a model [38] proposed for ices Ih and Ic, the latter type of bonds is

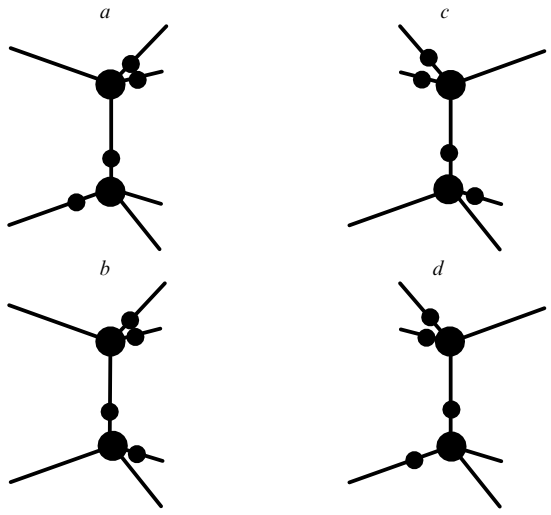


Figure 2. Types of hydrogen bonds in ices Ih and Ic: strong (*a*) and weak (*b*) hydrogen bonds between the hexagonal layers of ice Ih; strong (*c*) and weak (*d*) hydrogen bonds within a hexagonal layer in ices Ih and Ic.[38]

referred to as strong bonds, whereas the former type of bonds is referred to as weak bonds with the respective difference in the force constants used for their description. The application of this model to the interpretation of INS spectra of various crystalline ices is discussed in Section IV.

Within the model of two force constants, a structure with the maximum fraction of strong H-bonds has to be the most stable at a given geometry of the oxygen framework. Kirov [39] suggested a proton distribution over the structure of ice Ih containing only strong H-bonds. In this structure, the positions of protons are disordered in the hexagonal layer but are ordered along the *c* axis.[39] Analogous models comprising only strong H-bonds have also been suggested for ice Ic.[40,41] One of them is disordered along the direction [111] of the cubic lattice but contains ordered layers; another represents a defectless axial twin with a step-like proton ordering. However, it has to be noted that the proton-ordered ice Ic, even if observed, existed only as partially polarised thin films [42] on a support inducing this polarisation (see below in this Section), and the real proton-ordered crystal structure of ice XI comprises three weak H-bonds per strong H-bond. Thus, as mentioned above, it is the change in the geometrical parameters, in particular, relative shifts of hexagonal layers, that plays the decisive role in the stabilisation of the proton-ordered structure of ice XI rather than the fraction of strong bonds (calculated within the model of two force constants).[35,36]

It has been shown that partial proton ordering in an ice structure leading to its polarisation can be caused by surface effects. In particular, proton ordering resulting in a polarised structure was observed in thin films of ice Ih (1–80 monolayers) prepared by vacuum deposition of water vapour on a Pt(111) support at 137 K.[43] The strains occurring in the first monolayer due to mismatch between the cell parameters of platinum and ice Ih are relieved already at the fifth monolayer. The preferred orientation of the first H_2O monolayer lying on the Pt(111) crystal face induces the polarised ordering in subsequent layers. The extent of the orientation order decreases with an increase in the distance to the platinum surface (by a factor of ~ 2.7 at a distance of 30 monolayers).

Iedema *et al.*[42] reported partial polarisation of thin films of ice Ic (with thicknesses of 2000 to 100 000 monolayers) prepared similarly by the deposition of water vapour on a Pt(111) support at temperatures from 135 to 145 K. The degree of ordering in the films was 0.2% but it was independent of the distance to the support, in contrast to the data cited above.[43] The oxygen atoms of the H_2O molecules were directed away from the support. In both studies [42,43] it was considered that the partial ordering during ice crystal growth emerged due to interactions between the water molecules at the interface with the support or with the surface of the growing crystal.

Recently, the process of water freezing in narrow pores of glassy silicates, which is strongly affected by hydrophilic pore walls, has been elucidated. It was found [10] that water can be overcooled down to -18 and -27 °C in completely filled pores with diameter of 50 Å and in half-filled pores (which corresponded roughly to three molecular layers adsorbed on the pore walls), respectively. Remarkably, no indication of crystallisation down to -196 °C was observed in quarter-filled pores, which corresponded to an H_2O monolayer on the wall. The temperature of nucleation of the crystalline phase depends on both the degree of pore coverage with water and the pore size: it decreases with a decrease in the pore size, *i.e.*, water can be overcooled to a lower temperature in a narrower pore.[11] In addition, in sufficiently narrow pores, ice Ih crystallises in the case of partial filling, whereas ice Ic crystallises in the case of complete filling.[10,11]

2. Ice II. Phase transition Ih → II

The formation of crystalline water ices II–X and XII requires elevated pressures, therefore, these phases are referred to as high-pressure ices.

Many of the high-pressure ices can be retained in the metastable state even at 1 bar. To this end, an ice sample prepared at the corresponding high pressure should be cooled to liquid nitrogen temperature and this temperature should be kept during the pressure release down to atmospheric pressure. Such metastable states of water are referred to as quenched ices. It is for recovered forms at atmospheric pressure that the crystal structures of various high-pressure ices have been determined. However, these measurements give no information on the changes in structural parameters (such as the extent of proton ordering, volume compressibility, tensor of elasticity constants, *etc.*) as a function of pressure and temperature. Recently, the structures of various crystalline ice phases have been studied at different pressures and temperatures within the regions of their thermodynamic stability and/or metastability.

The crystal structure of ice II was determined for the first time by Kamb [44] in 1964 using single-crystal X-ray diffraction on a recovered sample at atmospheric pressure. Ice II possesses a rhombohedral structure with hexagonal columns composed of alternating six-membered rings in the chair conformation differing from each other in the degree of flattening (Fig. 3) along the *c* axis of the hexagonal unit cell or along the direction [111] in the rhombohedral unit cell as the main structural elements. The more corrugated rings comprise water molecules with the O(1) atoms, whereas more flattened rings are composed of the water molecules with the O(2) atoms. Each column is surrounded by six other columns of the same type going parallel but shifted by 1/3 translation along the *c* axis. The cavity inside the columns has a diameter of about 3 Å, which thus can accommodate helium or neon atoms or hydrogen molecules.[45] The resultant non-stoichiometric solid solutions of inert gases or hydrogen in ice II matrix can also be considered as host–guest hydrates with the framework of ice II as the host and gas molecules as guests.

The presence of a dissolved gas changes substantially the thermodynamic parameters of ice. For instance, crystallisation of ice from water at a hydrostatic pressure of 0.28–0.50 GPa in an atmosphere of helium upon cooling to the freezing point of 250–270 K gives rise to ice II-based helium hydrates rather than to ices III and V, which are thermodynamically stable in this region of the phase diagram (see Fig. 1).[45–47] The crystal structure of the helium hydrate with ice II-derived water framework, which

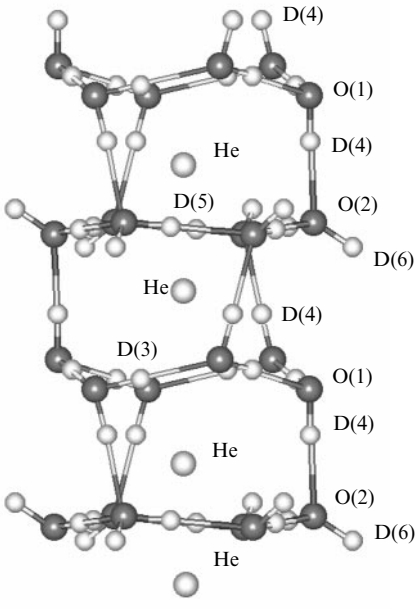


Figure 3. A hexagonal layer in ice II (the projection perpendicular to the *c* axis). Helium atoms that can penetrate into the hexagonal channels in ice II structure are also shown.

is formed under the above conditions, has been determined using powder neutron diffraction.[47] Like ice II, this helium hydrate is proton-ordered and this is the only known case when a proton-ordered crystalline framework of water molecules is formed directly from the liquid phase. The crystal structure of the gas-free ice II in the region of its thermodynamical stability has been determined for the first time by Lobban *et al.*[48] also using powder neutron diffraction; the results obtained made it possible to analyse the influence of absorbed gas on the geometry of the water framework of ice II.

Helium atoms in the hexagonal channels of ice II experience repulsion from the deuterium atoms D(4) at the oxygen atoms O(1) constituting the corrugated rings (see Fig. 3). As a result, helium atoms occupy positions closer to the flattened ring rather than exactly in the centre between the flattened and the corrugated rings within the unit cell of the respective hydrate (see Fig. 3).[47] The repulsion of the He atoms from the O(2) atoms of the flattened rings results in the increase in the diameter of these rings as compared to the structure of helium-free ice II.[48] Meanwhile, the diameter of the corrugated rings remains virtually unchanged. The inclusion of helium atoms into ice II structure results in the opposite changes in the unit cell parameters a and c.[48] The distance between walls of adjacent channels in the structure of the hydrate decreases due to the increase in the diameter of the flattened rings. Meanwhile, the distance between the axes of the channels somewhat increases upon inclusion of He, which results in the increase in the parameter a. In contrast, the parameter c somewhat decreases since the increase in the diameter of channels should be accompanied by the reduction in their lengths.

Upon an increase in pressure, the diameter of the flattened hexagonal rings changes insignificantly, whereas that of the corrugated rings decreases in both the structures of helium-free ice II and ice II-derived helium hydrate.[48] Upon an increase in pressure from 0.28 GPa to 0.48 GPa, the distance between the axes of the channels decreases. As anticipated, the volume compressibility of He-containing ice II is smaller than that of its helium-free prototype. An estimate[48] of the isothermal volume compressibility of pure ice (D_2O) at 200 K (14.8 GPa) is in good agreement with the value of 14.4 GPa obtained earlier[49] based on acoustic measurements for ice II(H_2O) at 237.5 K.

The structure of the water framework in ice II (free of dissolved helium) was simulated within the density functional theory using the PW91 functional at different temperatures and pressures.[50] The calculated values of density, volume compressibility, unit cell parameters and atomic coordinates were in good agreement with the experimental results.[44, 48, 49] The same simulations showed that the decrease in the density of ice II upon an increase in pressure is due to a decrease in the distance between the axes of the hexagonal channels, which is also in accord with the experimental observations.[48]

In an earlier study on the structure determination of quenched ice II, Kamb[44] noted that this structure can be derived from that of ice Ih by preserving some of the hexagonal channels of ice Ih while rearranging the system of H-bonds between them. This is accompanied by certain increase in the diameter of the hexagonal rings with a concomitant decrease in the distance between the axes of these channels, which gives rise to an increase in the density of the resultant framework. A scheme of such a conversion from the structure of ice Ih to that of ice II is depicted in Fig. 4.[51]

The transition of ice Ih to ice II under hydrostatic compression in an atmosphere of helium was studied experimentally using neutron diffraction.[52] The incorporation of helium atoms into ice Ih starts at 120 K at a pressure interval from 0.25 GPa to 0.31 GPa. This results in an expansion of the crystal lattice around the inserted helium atoms, which manifests itself in an increase in the distance between the (hh0) planes. Heating of the sample to 180 K at 0.31 GPa is accompanied by an abrupt phase transition of ice Ih with dissolved helium into ice II-based helium hydrate. Due to the large difference in densities of ices Ih and II, a single crystal of Ih converts into polycrystalline powder of ice II-based helium hydrate. It is of note that the positional proton disorder in the structure of ice Ih is preserved until completion of the transition into He-containing ice II.

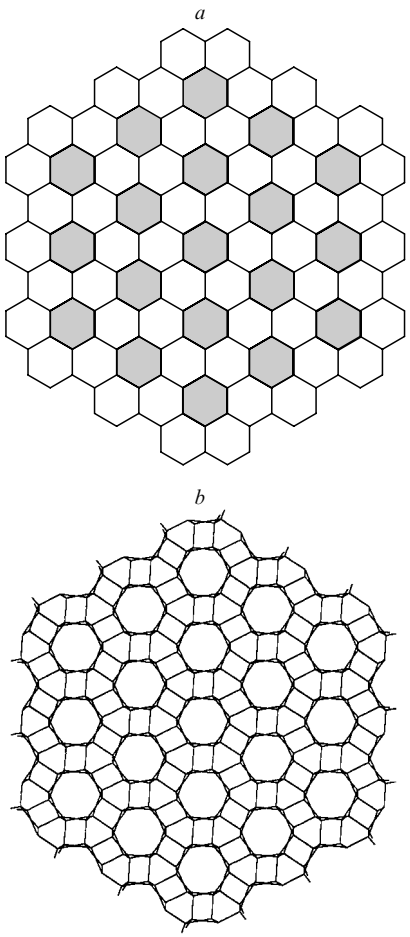


Figure 4. Rearrangement of the framework of hydrogen bonds of ice Ih (*a*) to ice II (*b*). In both cases, projections along the c axes of the hexagonal lattices are given. The hexagonal channels in ice Ih that are retained upon the transition Ih → II are marked grey.

3. Ices III and IX. Transition III → IX

The structures of ices III and IX at pressures from 0.28 to 0.30 were first determined by Londono *et al.*[53] using powder neutron diffraction. Later, powder neutron diffraction was applied to refine the structure of ice III in different points in the region of its thermodynamical stability.[54] Ices III and IX possess identical oxygen frameworks but differ from each other in the extent of proton ordering (Fig. 5). Gradual ordering of proton positions upon cooling of ice III compressed to 0.23 GPa in a temperature range from 208.0 to 164.5 K was established back in 1968 by dielectric susceptibility measurements.[2] The maximum change in the dielectric susceptibility as a function of temperature (which corresponded to the maximum ordering) was observed at ~173 K. Meanwhile, there was no indication of any changes in the oxygen famework. Thus, ice IX represents a low-temperature proton-ordered analogue of ice III.[2] It is of note that quenched ice III cannot be recovered at atmospheric pressure using the standard method since it always undergoes a phase transition to ice IX upon cooling. In the crystal structure of recovered ice IX determined[55] at atmospheric pressure using single-crystal neutron diffraction, the mean occupancy of the least occupied hydrogen position was as low as 4%. The change in entropy due to the phase transition III → IX was found[56] to be 1.34 ± 0.29 J K^{-1} mol^{-1}. Meanwhile, the theoretical value of the entropy change assuming the complete proton disorder in ice III and complete order in ice

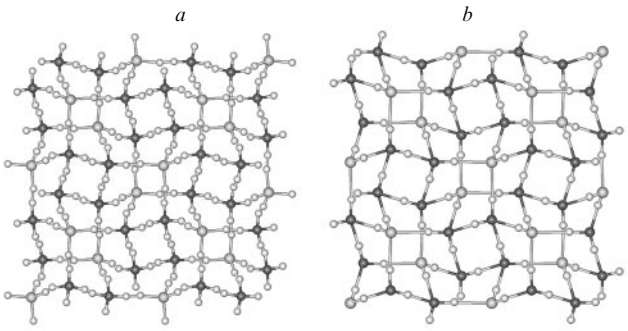


Figure 5. The structures of proton-disordered ice III (*a*) and its proton-ordered analogue, ice IX (*b*). The projection is along the *c* axis. All possible positions of the hydrogen atoms in ice III are shown; their occupancies are close to 0.5. The atoms O(1) forming helices along the *c* axis are marked black, whereas the atoms O(2) linking the helices into a united framework are marked grey.

IX should be 3.37 J K^{-1} mol^{-1} (Ref. 54), which is 2.5 times larger than the above experimental value (see Ref. 56). This large discrepancy cannot be explained solely by a partial proton disorder of ice IX, therefore, it was suggested that the structure of ice III is partially proton-ordered. The correctness of this suggestion was confirmed experimentally by crystallographic studies of ice III.[53, 54]

The mean occupancies of the least occupied proton position in the crystal structure of ice IX at 0.28 GPa and at atmospheric pressure are nearly the same (4%).[53] No substantial changes in the extent of positional proton order of ice III within the region of its thermodynamical stability were observed (the occupancy of the least occupied position was slightly larger than 40%).[54] However, the change in the configurational entropy due to the transition III → IX estimated from the occupancies of the proton positions in ices III and IX also exceeds the experimental value. Therefore, ΔS corresponding to this phase transition is not governed exclusively by the change in the configurational entropy due to different proton ordering in these phases, some other factors are also involved.[54]

In addition to the proton ordering, cooling of ice III is accompanied by changes in the unit cell parameters *a* and *c* and, consequently, the unit volume. It is of note that the relative decrease in the volume of ice due to the transition III → IX is an order of magnitude larger than that due to analogous transitions into proton-ordered phases with the conservation of the oxygen framework, *i.e.*, Ih → XI and VII → VIII.[53] The *c*/*a* ratio in ice III is larger than that in ice IX.[53, 54] Although the unit cell parameters *a* and *c* do not depend on the sample prehistory, both a decrease in temperature and an increase in pressure, on the whole, result in the anisotropic compression of ices III and IX with the parameter *c* decreasing faster than *a*. In addition, ice IX anisotropically expands upon pressure release to atmospheric pressure. In the crystal structures of ices III and IX, water molecules with the oxygen atoms O(1) form helices along the *c* axis, whereas water molecules with the oxygen atoms O(2) link the adjacent helices into a united framework (see Fig. 5). The ease of compression and stretching of the helices along their axes explains the lower rigidity of the parameter *c*.[54]

4. Ice V

In contrast to the transition of proton-disordered ice III into nearly completely proton-ordered ice IX, which does not violate any symmetry operations and thus preserves the space group $P4_12_12$, the proton ordering in the structure of ice V has to result in lower space symmetry of the crystal structure. According to structural studies of ice V at different temperatures and pressures (in particular, within the region of its thermodynamical stability) performed for the first time by Lobban *et al.*,[54] the degree of proton ordering in ice V generally increases upon cooling or compression. Nevertheless, no complete ordering is achieved. Thus, neither the aforementioned lowering of the space symmetry occurs, nor consequently changes in the space group are observed.[54] The crystal structure of receovered ice V at atmospheric pressure [57] corresponds to the same space group $A2/a$ as at 0.4 – 0.5 GPa.[54]

The O···O···O angles in the crystal structure of ice V (from 86° to 132°) deviate strongly from the bond angle H–O–H of a free water molecule (*ca.* 105°), which results in bending of the O–H···O hydrogen bonds. Straight hydrogen bonds are energetically more favourable than bent ones. Therefore, the fraction of H_2O molecules occupying unfavourable positions with strongly bent H-bonds in the crystal should decrease upon cooling thus increasing the degree of the orientational order of the structure.

On the one hand, an increase in pressure deforms the water framework (further distortion of the hydrogen bonds), while, on the other hand, the density of the phase increases, *i.e.*, the volume per water molecule in the crystal structure diminishes. The latter factor enhances the contribution of van der Waals repulsion, which tends to orient adjacent molecules that are not linked through H-bonds. Apparently, this factor is responsible for the proton ordering upon an increase in pressure, since the energy change due to the former factor is insignificant, as evidenced by theoretical estimates.[54]

The dielectric relaxation spectra [58] of ice V agree well with the observed proton ordering. The increase in the dielectric susceptibility of ice V upon cooling from 266 to 133 K amounts to 77% of the value calculated from the decrease in both volume and internal energy. Johari and Whalley [58] assign this difference to partial orientational ordering of H_2O molecules upon cooling.

Specific endothermic effects observed in the differential scanning calorimetry (DSC) curves (heating rate, 30 K min^{-1} at atmospheric pressure) for samples of metastable ice V subjected and not subjected to annealing at sufficiently high temperature can also be interpreted as a kinetic activation of the orientational transition proton order – disorder.[59] When ice V is cooled at a certain rate (say, 30 K min^{-1}), the orientational relaxation time required to achieve the equilibrium state becomes, starting from a specific threshold temperature, longer than the duration of the experiment. This results in kinetic freezing of the excessive proton positional disorder at low temperature. In subsequent heating at the same rate, the response of the system to heating is somewhat delayed since the orientational mobility of water molecules is initially too low, *i.e.*, at any given temperature *T*, the extent of proton disorder in the system is higher than the equilibrium value. With a further increase in temperature, the orientational mobility of molecules increases and, starting from a certain temperature, becomes sufficient to enable complete relaxation to the equilibrium degree of disorder. This is equivalent to the reactivation of the transition order – disorder related to the positions of protons in the structure of ice V.

The actuation of the orientational relaxation to the thermodynamic equilibrium is manifested in the DSC curves [59] registered at a heating rate of 30 K min^{-1} as an endothermic effect with a leading edge at 130 K and a width of 20 K for samples of ice V not subjected to annealing at sufficiently high temperature or with a leading edge at 125 K and a width of also around 20 K for preannealed samples or samples being heated for the second time. The orientational relaxation times τ for the structure of ice V at atmospheric pressure estimated from the DSC curves [59] are about 70 s and 7 s at 130 K and 140 K, respectively. These values are in accord with other estimates of τ for ice V at pressures of 0.50 GPa [54] and 0.61 GPa.[58]

5. Ices VI, VII, VIII and X and transitions between them

General features of the crystal structures of ices VI, VII and VIII (including the extents of the proton ordering therein) in the

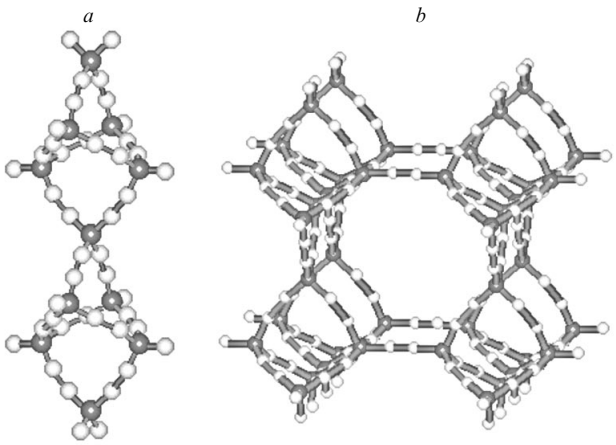


Figure 6. The structure of one of two identical independent interpenetrating frameworks of ice VI.
(*a*) The chain of water molecules stretched along the *c* axis representing the main structural unit in ice VI, (*b*) the pattern of assembly of the chains into the unied framework.
Chains forming the second framework (not shown here) pass through the cavities of the first framework. All possible positions of the hydrogen atoms are shown; the occupancies are equal to 0.5.

regions of their thermodynamical stabilities were determined in the mid-1980s.[60–62] Ice VI is composed of two identical independent interpenetrating water frameworks that represent structural analogues of the aluminosilicate framework $(Al,Si)O_2$ found in the mineral eddingtonite (Fig. 6).[60,63] According to the available data,[60] the structure of ice VI is completely proton-disordered throughout the region of its thermodynamical stability, no indication of any proton ordering has been revealed upon cooling. The crystal structures of ices VII and VIII can be described as two interposed frameworks of ice Ic. As a first approximation, one can consider that the oxygen atoms occupy the sites of a body-centred cubic (bcc) lattice of ice VII. Ice VII is completely proton-disordered,[60,61] whereas, in contrast, ice VIII is completely proton-ordered.[60,62] In the structure of ice VIII, the dipole moments of all molecules of the two independent frameworks of ice Ic are oriented along the directions [001] and $[00\bar{1}]$ of the tetragonal lattice. This results in the compensation of the dipole moments of both the independent frameworks in any unit cell of ice VIII. The interaction of molecules with oppositely oriented dipole moments gives rise to a relative shift of the frameworks along the *c* axis by 0.27 Å, which slightly distorts the bcc packing of oxygen atoms. Due to the shift, two distances between any oxygen atom and its four non-H-bonded neighbours appear longer (3.32 Å) and two appear shorter (2.74 Å) than the other four distances with the H-bonded O atoms (2.89 Å).[60,62] Ices VI, VII and VIII can be considered as self-clathrates owing to the presence of two interpenetrating water frameworks with no common hydrogen bonds in their structures.

In contrast to the transition III → IX (see Section III.3), the transition between ices VII and VIII is clearl and reversible, the conversion VII → VIII occurring at a temperature about 10 K lower than the reverse conversion VIII → VII.[60,64] Densities of ices VII and VIII at identical temperatures in the region of the transition are very similar.[60]

According to data from powder neutron diffraction,[60,62] the O–D covalent bond lengths and D–O–D bond angles in water molecules constituting ice VIII (0.97 Å and ~105°, respectively) are close to those in a free molecule[1] (0.958 Å and 104.5°, respectively). At the same time, refinement of the structure of ice VII using the neutron diffraction data under assumption of oxygen atoms occupying sites of the bcc lattice yields unrealistically short O–D distances of 0.89 or 0.943 Å (see Refs 60, 61) and unrealistically large D–O–D angles of 109.5°. This was rationalised as disordering of the equilibrium positions of either oxygen atoms around the sites of the bcc lattice with a deviation $\delta(O)$[60] or deuterium atoms around the positions (x,x,x)[61] with a deviation $\gamma(D)$. Refinement of these models afforded more realistic O–D bond lengths and D–O–D bond angles; however the best-fit deviations $\delta(O)$ and $\gamma(D)$ did not exceed the respective thermal vibration amplitudes.[60,61] Therefore, several new attempts aimed at the redetermination of the crystal structures of ices VII and VIII have been undertaken.

Nelmes *et al.*[65] elucidated the structures of ices VII and VIII at identical *P* and *T* with pressures ranging from 3.3 to 20.6 GPa and in temperature intervals lying between the transitions VII → VIII and VIII → VII (*i.e.*, under the conditions admitting the coexistence of both phases) using neutron diffraction. For ice VII, the atomic parameters were refined within three different models of deviations of O atoms from the sites of the bcc lattice: (i) six possible positions for a deviation along the family of symmetrically related directions ⟨100⟩, (ii) twelve positions for a deviation along the family of directions ⟨110⟩ and (iii) two sets of four positions forming a regular tetrahedron for a family of directions ⟨111⟩ or $\langle\bar{1}\bar{1}\bar{1}\rangle$. For the D atoms, three different models of deviations from the equilibrium positions perpendicular to the directions ⟨111⟩ were also considered: (i) three positions $(x+u, x, x)$, $(x, x+u, x)$ and $(x, x, x+u)$, where $u = \gamma/\sqrt{2}a$; (ii) three positions $(x-u, x, x)$, *etc.* and (iii) six positions $(x+v, x-v, x)$, *etc.*, where $v = \gamma/\sqrt{6}a$, *a* is the cubic lattice parameter. After the refinement of atomic positions, those combinations of possible O and D sites were chosen that gave the O–D distance and D–O–D angle closest to the mean values for ice VIII at the same *P* and *T*. The model of disordering of O atoms around the sites of the bcc lattice along the directions ⟨111⟩ and of D atoms over three positions $(x+u, x, x)$, *etc.* provided the maximum likelihood. Within this model, the mean O–D bond length [0.977(7) Å] and the D–O–D bond angle [107(1)°] in the structure of ice VII at 5.1 GPa appeared very similar to the respective values in the structure of ice VIII (0.97 Å and 107.3°, respectively). Due to the deviations of O positions from the sites of the bcc lattice, the structure of ice VII reveals two types of hydrogen bonds with lengths of ~2.75 and ~2.93 Å.[65] With an increase in pressure to 20.6 GPa, the O–D bond lengthens to 0.98 Å (ice VIII, 230–250 K) and 0.99 Å (ice VII, 260–280 K).[65]

Systematic investigations into the structure of ice VIII using powder neutron diffraction at a pressure ranged from 2 GPa to 10 GPa at 265 K confirmed[66,67] the tetragonal crystal structure with one independent oxygen and one deuterium atoms in the positions $(0, 1/4, z)$ and $(0, y, z)$, respectively. Furthermore, it was found that the O–D covalent bond linearly elongates with an increase in pressure and the relative shift ε between the two independent frameworks of hydrogen bonds decreases with an increase in pressure (rapidly and non-linearly in the range from 2 GPa to 3 GPa and linearly in the range from 3 GPa to 10 GPa).

Ice VIII is thermodynamically stable above 2 GPa. However, at temperatures below 125 K, the ice VIII structure is retained with pressure release. It was established that many properties of this phase (in particular, positions of bands in the Raman spectra[68]) change non-linearly in the pressure range from 2 GPa to atmospheric pressure. The same is true for the frequencies of translational vibrations revealed in INS[68] and IR spectra.[68,69] Neutron diffraction studies of ice VIII at 85 K at a pressure from 7 GPa to 0 GPa demonstrated[68] that this non-linearity was due to a drastic increase in the relative shift ε between the independent water frameworks in the structure of ice VIII with a decrease in pressure owing to a weakening of the electrostatic interaction between them. For a constant temperature of 85 K, the non-linear increase in ε with an increase in pressure starts at 7 GPa and ceases at ~1 GPa.[68] As mentioned above, at 265 K, this transition starts

between 3 GPa and 2 GPa but is interrupted at a lower pressure by the subsequent transition VIII → VI.[66,67] Besson *et al.*[68] explained this abrupt weakening of the electrostatic interactions between the independent water frameworks in the structure of ice VIII with a decrease in pressure by a respective drastic change in the charges on the O and D atoms, which should give rise to strengthening of the covalent O–D bond and, respectively, to its shortening. Indeed, according to the available experimental data, the O–D bond length in the structure of ice VIII decreases with a reduction of pressure.[68]

In contrast to ice VIII, the quenched form of ice VII (like that of ice III) cannot be recovered at atmospheric pressure by the standard methods, since it always transforms into the ordered ice VIII upon cooling. This transition occurs at about 273 K at a pressure from 2 GPa to 15 GPa. Notwithstanding, a new low-temperature metastable form of ice VII existing within the region of stability of ice VIII has recently been discovered; this can be prepared by isothermal compression of various crystalline ices or high-density amorphous ice (HDA) below 150 K. Quenched ice VII can be recovered at atmospheric pressure from this form by pressure release at low temperature.

This low-temperature metastable form of ice VII is often referred to as ice VII′. This form has been prepared for the first time by isothermal compression of ice Ih at 77 K (see Ref. 70). First, the transition Ih → HDA occurs at 1.0 GPa (it is considered in detail below in Section III.6 devoted to amorphous ices), then HDA converts into ice VII′ at ∼4 GPa. Ice VII′ transforms into ice VIII upon isobaric heating. Different ice phases were identified by Raman spectroscopy.

A transition of ice VI(D_2O) into ice VII′ was also observed.[12] Ice VI was prepared by cooling liquid D_2O down to 300 K at 1.5 GPa. Then the temperature was further lowered to 95 K and ice VI was compressed to 5.4 GPa. During compression, an abrupt increase in pressure was observed at $P = 3.8$ GPa, which can be interpreted as a transition into a new phase. According to neutron diffraction data, this phase has a structure of ice VII, which is conserved after the isothermal (at 100 K) release of pressure down to atmospheric pressure. A neutron diffraction study of recovered ice VII′ at $P = 1$ bar confirmed that this is identical with ice VII. Storage of ice sample at atmospheric pressure at 77 K did not result in any structural changes, as was also evidenced by neutron diffraction.[12]

The compression of ice II at low temperatures also affords a metastable phase with the structure of ice VII.[71] In contrast to ice VII′ prepared from ice VI, diffraction patterns of ice VII′ samples prepared from other ices revealed some features not typical of pure ice VII. Meanwhile, the IR and Raman spectra of the differently prepared ice VII′ samples were identical.[70,71]

Song *et al.*[71] determined the boundaries of the metastability region of the low-temperature phase VII′. In that study, ice VII′ was produced by isothermal compression of ices II and VI to 4–10 GPa below 120 K. Ice phases were identified by IR spectroscopy. The compression of ice VI in the temperature range of 200–273 K leads to a transition into ice VIII at 1.9–2.1 GPa. On the other hand, no conversion into ice VIII is observed upon isothermal compression of ice VI at $T < 150$ K, which is near the boundary between the stability regions of ices VI and VIII as estimated by the extrapolation of its experimentally established high-temperature part. Further increase in pressure induces the transition into ice VII′. The pressure of the transition VI → VII′ increases with a decrease in temperature: from 2.8 GPa at 120 K to 7.9 GPa at 40 K. Similar trends were also reported for the compression of ice II (see Ref. 71) and HDA.[70] Further increase in pressure at a temperature below 100 K results in the transformation of ice VII′ prepared by the method described above into ice VIII at 30 GPa irrespective of temperature. The isobaric heating of ice VII′ also induces the transition into ice VIII, the temperature range of this transition is from 10 to 20 K, and the temperatures of the start and completion of this transition decrease with an increase in pressure. Thus, metastable ice VII′ exists in the pressure range from 2.8 GPa to 30 GPa at temperatures below 180 K.

The temperature-induced transition of ice VII′ into the ordered state proceeds[71] due to the activation of the orientational mobility, which allows rearrangement of water molecules into ice VIII, *i.e.*, the phase with a higher thermodynamical stability. The VII′ → VIII transition upon isothermal compression at temperatures below 100 K is due to rotational tunneling of water molecules, because their rotational mobility is frozen under the conditions indicated. The probability of a tunnelling jump is determined by the lengths of the hydrogen bonds, which strongly depend on pressure and are virtually independent of temperature under the conditions considered. Thus, the pressure of the transition VII′ → VIII initiated by the isothermal compression at $T < 100$ K is also virtually independent of temperature.[71]

With an increase in pressure, the structures of ices VII and VIII gradually change, which finally results in the formation of a new crystalline framework phase, *viz.*, ice X, where the oxygen atoms form a bcc lattice (as in the structure of ice VII) with hydrogen atoms residing exactly in the middle between the respective oxygen atoms.

In the structures of ices VII and VIII, the distances between oxygen atoms both connected and not connected by H-bonds decrease with an increase in pressure. This impedes rotation of water molecules due to, first, strengthening of the H-bonds and, second, steric repulsion of non-H-bonded adjacent oxygen atoms. Therefore, an increase in pressure suppresses orientational mobility of water molecules as regards their rotation around the oxygen atoms. In parallel, another mechanism of proton positional disordering is becoming increasingly important. The approach of the oxygen atoms linked by the O–H···O bonds decreases the distance between two minima of the potential energy corresponding to two possible positions of an H atom along this bond. Simultaneously, the barrier height between them is decreased thus increasing the frequency of proton tunnelling transitions between these two minima. In the case of proton-ordered ice VIII, this should bring about disordering of proton positions, *i.e.*, to a transition into ice VII. In addition, such transitions lead to the dissociation of water molecules to form defects, such as H_3O^+ and OH^-. When the probability of occurrence of a proton exactly in the centre of the respective O···O bond becomes equal to those in the minima of the potential energy along this hydrogen bond, ice VII transforms into a new form with symmetric hydrogen bonds, *viz.*, ice X. With further shortening of the distance between the oxygen atoms, the probability density of the proton localisation in a given point will have a single maximum at the centre of the bond. Furthermore, the two potential energy minima along the O–H–O bond coalesce, which all the more retains the symmetry of the H-bond.

The idea that the O–H···O hydrogen bond should become symmetric with a single potential energy minimum at an elevated pressure was proposed more than 30 years ago.[72] An alternative definition of the symmetric hydrogen bond was suggested: a hydrogen bond is considered symmetric provided that the distribution function of proton positions along the hydrogen bond has the only maximum exactly at its centre.[73] The structures with two potential energy minima but one maximum of the proton distribution function exactly at the centre of the O···O bond are referred to as proton-disordered symmetric ices, whereas those with the single potential energy minimum at the centre of the hydrogen bond are referred to as proton-ordered symmetric ice.[74]

The sequence of structural changes occurring with ices VII and VIII with an increase in pressure described above was fully supported by quantum-chemical calculations.[74–76] In the calculations, the molecular dynamics method was used with atomic nuclei treated within the quantum mechanical approximation.

The simulation box contained sixteen water molecules. The simulation was performed in the *NPT* ensemble.† No dimensionality reduction or other approximations, including quasiclassical and quasiharmonical, apart from the neglect of exchange between identical species were applied in the calculation of the path integrals. For each specific configuration, the forces experienced by nuclei were calculated within the Born–Oppenheimer approximation based on the electronic structures determined within the density functional theory. The simulation admitted cleavage and reformation of chemical bonds.

The following sequence of transitions as a function of increasing pressure was revealed for 100 K: ice VIII–ice VII (owing to tunnelling translational transitions of protons along the hydrogen bonds)–proton-disordered ice X–proton-ordered ice X.[74] The pressure required for the transition of ice VII(H_2O) into the structure with two potential energy minima for a proton along the hydrogen bond and a single maximum of the proton distribution function located in the centre of the bond was estimated [76] to be 55 GPa at 300 K. The pressure of the next transition into ice with a single potential energy minimum in the centre of the hydrogen bond was estimated to be 110 GPa at the same temperature.[76]

The implementation of diamond anvil cells over the last decades has made it possible to generate ultrahigh pressures and characterise samples subjected to extreme conditions by various spectroscopic techniques and X-ray diffraction. In particular, Hemley *et al*.[77] used X-ray diffraction with synchrotron radiation (SR) to show that oxygen atoms still occupy the sites of the bcc lattice up to a pressure as high as at least 128 GPa. A more recent SR-based single-crystal X-ray diffraction study of ice VII(H_2O) at 300 K and pressures up to 170 GPa demonstrated [78] that the oxygen framework of ice VII is preserved under these conditions and the hydrogen bonds become symmetric in the pressure range from 60 GPa to 150 GPa. Although the localisation of hydrogen atoms based on X-ray data is challenging, the proton ordering in the cited study was monitored by the intensity of reflection (111) and its symmetry equivalents, which are forbidden in the ideal bcc structure with fully disordered proton positions. With an increase in pressure, the intensities of these reflections first increased, then reached a plateau at 60 GPa and then again started to increase rapidly after 150 GPa. This is in agreement with two theoretically predicted [74–76] transitions of ice VII first to the proton-disordered and then to the proton-ordered ice X, for which these reflections are allowed.

More direct evidence for the symmetrisation of the hydrogen bonds can in principle be provided by neutron diffraction, which can reliably locate positions of deuterium atoms. However, these experiments under ultrahigh pressures are presently not feasible since they require relatively bulky samples taking into account the low neutron-scattering cross-section. As mentioned above, neutron diffraction studies on the structures of heavy ices VII(D_2O) and VIII(D_2O) in the pressure range up to 20 GPa revealed some increase in the length of the O–D covalent bonds.[66,67] This experimental observation is also supported by the results of quantum-chemical calculations.[76]

The transitions of ices VII and VIII into the form with the symmetric hydrogen bonds can also be monitored by means of vibrational spectroscopy, since three types of bands corresponding to the three types of vibrations of a water molecule in a molecular crystal should be transformed into two types of bands typical of a framework crystal. According to the IR studies of ice VII(H_2O) at room temperature in the pressure range up to 110 GPa, the symmetrisation of the hydrogen bonds occurs between 59.5 GPa and 64.7 GPa.[79] In a more detailed IR study [80] of ices VII and VIII (both H_2O and D_2O) at temperatures between 85 K and 300 K in the pressure range up to 210 GPa, the transition to the symmetrically H-bonded structure was found to occur at 60 GPa (H_2O) and 70 GPa (D_2O). In both cases, the transitions afforded proton-disordered ice X and the experimentally measured transition pressures agreed well with the respective theoretical estimates.[76] In addition, Goncharov *et al*.[80] reported changes in the IR spectra at a pressure between 150 GPa to 160 GPa, which suggests the subsequent structural transition to the proton-ordered ice X devoid of proton tunnelling transitions between the two potential energy minima.

According to Raman studies [81] of ices VII, VIII and X at pressures up to 100 GPa, the transition from ice VII to ice VIII occurs at 273 K at pressures lower than 12 GPa, and the transition temperature rapidly decreases with an increase in pressure approaching 0 K at about 60 GPa. In another Raman study by Goncharov *et al*.,[82] the phase diagram of H_2O was determined in the regions of the transitions VII–VIII–X. The authors found that the transition into the proton-ordered ice X with the symmetric H-bonds occurs at $P > 100$ GPa.

The phase diagrams of ices H_2O and D_2O in the regions of the transitions VII–VIII, VII–X and VIII–X were also systematically elucidated by Song *et al*.[83] using IR spectroscopy. The transition to the proton-disordered ice X with the symmetric H-bonds was monitored in the temperature range of 12–298 K and pressure range of 2–100 GPa. The transition VII–VIII occurred at about 273 K for H_2O (at 277 K for D_2O) at a pressure of $\sim$15 GPa, and the transition temperature decreased nearly linearly as a function of pressure down to $\sim$100 K at 62 GPa (H_2O) and 75 GPa (D_2O). The values of pressure where the transitions VII–X and VIII–X occurred depended little on temperature: in the case of H_2O, the transition pressure increased only from 60 GPa to 62 GPa on going from 300 K down to 12 K; in the case of D_2O, the transition pressure increased from 72 GPa to 77 GPa on going from 298 K down to 16 K. The determined [83] temperatures and pressures of the transitions VII–VIII–X were in good agreement with the respective values obtained earlier using IR [79,80] and Raman [81,82] spectroscopy. The triple point VII–VIII–X was located at 100 K and 62 GPa for H_2O and at 100 K and 75 GPa for D_2O.[83] According to theoretical predictions,[74–76] the isothermal compression of ice VIII between 100 K and 273 K should first initiate the transition to ice VII and then to ice X.

Schwager *et al*.[84] determined the melting curve of ices VII(H_2O) and X(H_2O) in the pressure range from 20 GPa to 90 GPa. The curve revealed a kink around 43 GPa supposedly attributed to the triple point VII–X–liquid (at 43 GPa and 1600 K). The dissociation of H_2O molecules in the liquid phase became significant only at temperatures above the melting point by 200–400 K.[84]

It is of note that the symmetrisation of hydrogen bonds upon the transition VII $\rightarrow$ X switches the mechanism of proton diffusion in the crystal. In the structure of ordinary ice, the diffusion proceeds in two steps (a proton can move to the adjacent energy minimum along the H-bond or jump to a different bond) but in the case of ice with the symmetric H-bonds, the diffusion can be accomplished only by jumps between the bonds. Thus, it might be expected that the proton diffusion coefficient of ice X is higher than that of ice VII. Furthermore, compression of ice VII increases the concentration of ionic defects, which should also lead to an increase in the proton diffusion coefficient with an increase in pressure. However, direct measurements of the proton diffusion coefficient for ice VII at pressures ranged from 10.2 GPa to 63 GPa at 400 K (which lies in the region of its thermodynamic stability) showed [85] that under these conditions the proton diffusion coefficient decreases from 10^{-15} m^2 s^{-1} to 10^{-17} m^2 s^{-1} with an increase in pressure.

† *NPT* ensemble is a thermodynamical ensemble in which the total number of particles N, pressure P and temperature T remain constant; other thermodynamical ensembles, *e.g.*, *NVE* (with the constant total number of particles N, volume V and total energy E) and *NVT* (with the constant total number of particles N, volume V and temperature T) will be referred further in the text.

6. Kinds of amorphous ices. Pressure-induced amorphisation of crystalline ices and crystallisation of different ices from amorphous water phases on heating

As has been mentioned above, the isothermal compression of ice Ih affords HDA, which in turn transforms into crystalline ice VII′ upon further compression. This example of interconversions of amorphous and crystalline ices is not unique. The kinds of amorphous ice known to date are considered in this section in their relation to crystalline ices.

Amorphous ice has been prepared for the first time by deposition of water vapour onto a copper support cooled to a temperature below 163 K (see Ref. 8). The density of amorphous ice produced in this way [86] was 0.94 g cm^{-3}. Sometimes, this type of amorphous ice is referred to as amorphous solid water (ASW). Rapid cooling of water emulsions composed of water droplets with sizes of the order of a few micrometers at a rate of more than 10^5 K s^{-1} affords amorphous ice of a similar density.[19] This form is typically referred to as hyperquenched glassy water (HGW). The thermodynamical properties of ASW and HGW are much alike and thus they can be considered as the same phase.[59] Upon heating, ASW and HGW convert into ice Ic, which in turn converts into ice Ih at higher temperature.

A detailed study of phases prepared by deposition of water vapour on a cold metal support has shown [86] that the type of the phase formed depended on the temperature and deposition rate. In particular, the deposition at a rate of 10 mg h^{-1} onto a support kept at 77 K affords amorphous ice with a density of 0.94 g cm^{-3}, whereas the deposition at a rate of 4 mg h^{-1} onto a support at 10 K yields another form of amorphous ice with a density of 1.1 g cm^{-3}. For the former case, according to wide-angle X-ray scattering, the local structure is characterised by nearly ideal tetrahedral environment of water molecules with the O$\cdots$O$\cdots$O angle close to 109° and the mean distance between the oxygen atoms of 2.76 Å. In the latter case, the mean closest distance between the oxygen atoms is also about 2.76 Å; however the overall local structure is more complicated than in the former phase. Therefore, the very slow deposition onto a very cold support (kept at a temperature below 55 K) affords amorphous ice other than ASW, which is characterised by higher density and distinct structural and thermodynamical characteristics.[86]

Mishima *et al.*[20] developed another method for the preparation of amorphous ice by isothermal (at 77 K) compression of ice Ih. Upon compression to $\sim$1.0 GPa, the volume of the samples gradually decreased, the decrease became abrupt in the pressure range from 1.0 GPa to 1.5 GPa and again smooth with a further increase in pressure to 1.6 GPa. When the pressure was isothermally (at 77 K) released to the atmospheric value, the sample expanded elastically, this was accompanied by a gradual increase in its volume. The densities of the sample were 1.31 g cm^{-3} and 1.17 g cm^{-3} at 1.0 GPa and atmospheric pressure, respectively. Ice sample prepared in this way proved amorphous, as evidenced by powder X-ray diffraction. Subsequent annealing of the sample at atmospheric pressure afforded another amorphous phase with a density of 0.94 g cm^{-3}. The heavier amorphous phase was referred to as HDA (see previous Section) and the lighter one to as low-density amorphous ice (LDA). Thermodynamical properties of LDA differ from those of ASW and HGW.[20, 59] LDA transforms into cubic ice Ic upon annealing, similar to ASW and HGW. Presently, there is no consensus on the equivalency of ASW and HGW on the one hand and LDA on the other.[59, 87] The relation of HDA to amorphous ice with a density of 1.1 g cm^{-3} produced [86] by the slow deposition on a cold support also remains a subject of debate.

Like ice Ih, LDA converts into HDA upon isothermal compression at 77 K, albeit the transition LDA $\rightarrow$ HDA starts at lower pressure (*ca.* 0.6 GPa) [21] than the transition Ih $\rightarrow$ HDA. It is of note that the transitions Ih $\rightarrow$ HDA and LDA $\rightarrow$ HDA are irreversible but have some common features with first-order phase transitions as regards stepwise changes in certain parameters.[20, 21]

The compression of ice Ic also yields HDA.[88] Therefore, the following closed loop of transitions can be realised: (i) Ic $\rightarrow$ HDA upon isothermal (at 77 K) compression to 0.8 GPa, (ii) elastic expansion of HDA by isothermal (77 K) pressure release down to atmospheric pressure, (iii) HDA $\rightarrow$ LDA by annealing at atmospheric pressure, (iv) LDA $\rightarrow$ Ic by annealing at higher temperature at atmospheric pressure.[88]

As has been mentioned in the previous section, HDA transforms into ice VII′ upon isothermal (at 77 K) compression to 4 GPa.[70] Meanwhile, the isothermal compression at higher temperature (*ca.* 140 K) initiates the transition of HDA into ice VIII. Upon isobaric heating, HDA can convert into various crystalline ices, depending on the pressure and heating rate. For instance, the transition of HDA into ices Ih (through the intermediate steps of LDA and Ic), VI and VIII at $T \leqslant 160$ K was reported.[70] Systematic studies of conversions of HDA in the course of isobaric heating at different pressures revealed that HDA transforms into LDA at $P \approx 0.2$ GPa [89] and, at higher pressures, subsequently into crystalline ice III′ ($\sim$0.2–0.3 GPa), a mixture of ices IV, V and XII ($\sim$0.4–0.7 GPa) and a mixture of ices VI and XII ($\sim$1.0–1.2 GPa).[90] The aforementioned crystalline ice III′ represents ice III with a higher degree of proton ordering, which transforms first into ice IX and then to ice II upon isobaric heating at $\sim$0.2–0.3 GPa. Some features of the transition [91] of HDA to ices IV and XII upon isobaric heating are discussed in more detail below.

The density of HDA increases in the course of isobaric heating at 1.1 or 1.9 GPa. If the heating of HDA is stopped before the start of crystallisation of ices IV or XII, a new amorphous ice phase with a density of 1.25 g cm^{-3} different from the phases described above can be recovered at atmospheric pressure by cooling the sample down to 77 K followed by pressure release at this temperature.[92] This phase is referred to as very high-density amorphous ice (VHDA). Upon heating at atmospheric pressure, VHDA is transformed directly to LDA without intermediate formation of HDA.[92] It is of note that the structures of HDA and VHDA determined at similar densities are very similar, therefore, VHDA probably should not be considered as an independent amorphous phase.[93]

Section III.8 considers yet another type of transitions between crystalline and amorphous ices, *viz.*, temperature-induced transformation of quenched ices VII′ and VIII into LDA.[12]

At present, the investigations into amorphous ices are focused on the following issues.

1. How different are the known amorphous water phases and what properties are the most indicative of this difference? In particular, what is the difference between the local structures of amorphous ices? What is the fundamental reason for water polyamorphism?

2. Which of the aforementioned amorphous phases can be considered as a thermodynamic extension of overcooled liquid water to the region of lower temperatures?

3. What are the thermodynamic characteristics of the transitions between amorphous ices? In particular, does the second critical point of water exist, which corresponds to the experimentally observed first-order LDA $\rightarrow$ HDA transition, and what are its P, T coordinates?

4. What is the mechanism of the pressure-induced amorphisation of ices Ih and Ic and whether such amorphisation is possible for other crystalline ices?

5. What is the mechanism of the solid-state crystallisation of amorphous ices upon annealing at 150–170 K?

A discussion of the above issues can be found elsewhere.[87, 94, 95] Ponyatovsky *et al.*[96] proposed a new method (alternative to the adopted method by Mishima and Stanley [94]) for the determination of the coordinates of the second critical point of water and applied it [97] to elucidate non-equilibrium phase diagrams of substances other than water. Non-equilibrium transitions between crystalline and amorphous water phases in the low-temperature part of the phase diagram were studied in detail

by Gromnitskaya *et al.*[98] and by Lyapin *et al.*[99] Very recently, Brazhkin and Lyapin [100] surveyed the experimental data on the transitions between disordered condensed phases (either liquid or solid) of various compounds and modern theoretical approaches to their description.

7. Ices IV and XII

Let us resume the discussion of properties of crystalline ices and transitions between them.

Some properties of ices Ic and IX, which have no specific regions of thermodynamic stability in the water phase diagram, have already been discussed above. In addition to these two forms, two more modifications, *viz.*, ices IV and XII, are also known to exist only in metastable state within the regions of stability of other ices.

The existence of metastable crystalline ice IV has already been mentioned in the very first studies [101, 102] of the water phase diagram. It was established that ice IV exists within the region of stability of ice V and can be prepared by overcooling liquid water in a certain pressure range.[4, 102] The structure of quenched ice IV recovered at atmospheric pressure at 10 K was determined by Engelhardt and Kamb [103] (Fig. 7). Structural parameters of ice IV were also reported for 210 K and 0.7 GPa, which lies within the region of its metastable existence.[90]

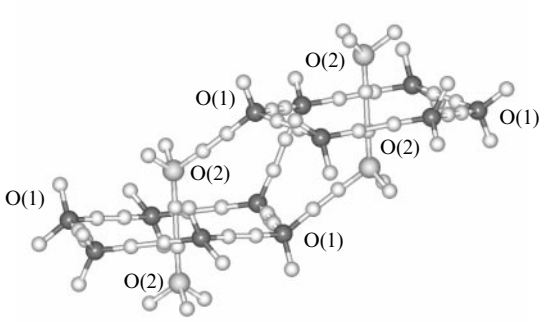


Figure 7. Two identical fragments of the structural motif of ice IV linked to each other. All possible positions of the H atoms (with the occupancies of 0.5) are shown.

Note that ice IV persisted at 248 K only for a short period from a few seconds to several minutes before spontaneous transformation into a more stable phase in a study [4] aimed at determining transition lines IV – VI and liquid – ice IV and the triple point liquid – IV – VI. In the study of the transition liquid – ice IV within the region of stability of ice V, the formation of other metastable crystalline ices was detected as well but it appeared impossible to reliably characterise them since the probability of their formation was even lower and their conversion into the stable phase proceeded even faster than for ice IV.[4]

A reproducible method for the preparation of one of these metastable crystalline phases, ice XII, was developed quite recently.[6] It consists of slow cooling of liquid D_2O in an argon atmosphere at 0.55 GPa and 260 K, *i.e.*, again within the region of stability of ice V. Under these conditions, the crystal structure of ice XII was determined (Fig. 8) and its density was measured, which appeared rather close to that of ice IV and somewhat higher than that of ice V.

Later on, the same phase was prepared [104] in a totally different region of the water phase diagram by isothermal compression of ice Ih to 1.8 GPa at $T < 150$ K, albeit it is HDA rather than crystalline ice that was produced under nearly the same conditions in previous studies.[20, 70] The reasons for the formation of ice XII instead of HDA remained unclear. Further investigations revealed [105] that the compression of Ih yields ice XII always through the intermediate formation of HDA. Ice XII crystallises only from LDA rather than directly from ice Ih and only at a

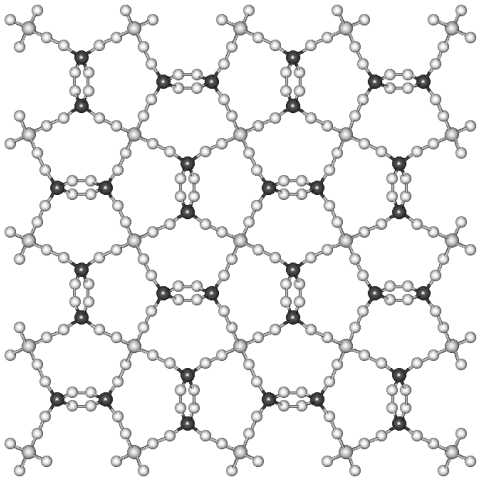


Figure 8. The structure of ice XII (the projection along the *c* axis). The occupancies of H positions are close to 0.5.

sufficiently high pressure and temperature. In particular, Koza *et al.*[104] found that ice XII was produced by the compression of ice Ih to $P > 1.1$ GPa at 77 K only in the case of imperfect mechanics operation giving rise to pressure drops, whereas no ice XII was formed in the case of smooth pressure trends. Likely, pressure drops result in acoustic pulses and consequent local heating of the sample up to 260 K, which actuates nucleation and growth of ice XII crystallites.[105] From the standpoint of these results, boundaries of the region of existence of ice XII determined by Koza *et al.*[104] required verification accounting for the pressure drops.

According to the study [3] of the transition HDA → XII → stable crystalline ice upon isobaric heating of HDA prepared by smooth compression of ice Ih at various pressures, the refined second region of existence of metastable ice XII lies within the region of stability of ice VI and extends from 158 to 212 K and from 0.7 to 1.5 GPa. Interestingly, the two regions of metastability of ice XII are disconnected, *i.e.*, there is no direct path to pass from one region to another avoiding phase transitions. In particular, ice XII prepared from liquid water at 260 K transforms [6] into stable ice V upon cooling, whereas ice XII prepared from HDA transforms [3] into ice VI upon heating above 212 K. It is of note that the temperature-induced transition of HDA to ice XII is much faster than the subsequent transition of ice XII to ice VI. Presumably,[3] the structure of HDA intrinsically contains crystallisation nuclei of ice XII.

Further analysis of properties of ice XII in comparison with those of ice V using DSC suggested [59] that some features of the DSC curves of ices XII and V can be explained by kinetic activation of the proton transition order – disorder resulting in partial proton ordering therein due to prolonged storage at 110 – 115 K. At the same time, the available neutron diffraction data [6, 104] strongly suggest the complete proton disorder in the structure of ice XII. Salzmann *et al.*[59] proposed the following explanation of this discrepancy. In one of the neutron diffraction studies,[6] the structure of ice XII was determined at 260 K, which is above the suggested transition order – disorder. In the second study,[104] ice XII was prepared at low temperature under the action of pressure drops. Rapid quenching of the sample heated by an acoustic pulse can in this case be responsible for the freezing of the positional proton disorder.

The measured [3] lower boundary of the region of existence of ice XII prepared from HDA is determined by kinetics of the transition HDA → XII and this type of ice XII can in principle be cooled down to extremely low temperatures. In particular, the structure of ice XII was determined at 1.5 K and atmospheric pressure.[104] (Those samples were produced from HDA at different

pressures; then the pressure was released to atmospheric pressure while the samples were cooled to 77 K, and finally the samples were cooled down to 1.5 K.) It was even suggested [3] that ice XII prepared by heating of HDA and existing within the region of stability of ice VI can become thermodynamically more stable than ice VI at low temperature. However, Johari [106] showed that the Gibbs free energy of ice XII at 1.1 GPa and 100 K is higher than that of ice VI thus confirming that ice VI is the stable phase.

In several cases, some amounts of ice IV formed upon annealing of HDA in addition to ice XII.[3] A more detailed study [91] of the crystallisation of HDA upon isobaric heating at $P = 0.81$ GPa up to 195 K at variable rates confirmed the possibility of the formation of ice IV. Under the conditions used, HDA converted into ices XII and IV simultaneously with the relative yields depending on the heating rate.[91] Pure D_2O ice IV and nearly pure H_2O ice IV were formed on slow heating at a rate of 15 K min^{-1}. Mixtures of ices IV and XII were obtained at intermediate heating rates. This means that both entirely metastable high-pressure ice phases, ices IV and XII, exist within approximately identical regions of the phase diagram and can be prepared by either crystallisation of overcooled liquid or temperature-induced crystallisation of metastable LDA.

It is of note that very soon after the publication of the neutron diffraction study of ice XII,[6] an independent report on the preparation of a new ice phase, unknown for that moment and crystallising from liquid water within the regions of stability of ices V and VI, appeared.[5] The authors determined the melting curve of the phase, described typical crystal morphology and measured Raman spectra but failed to assign it to ice XII, since very limited information on this modification was then available. Recently measured [107] Raman spectra of ice XII manifest pronounced similarity to the spectra of that unidentified phase [5] thus strongly suggesting that it was indeed ice XII.

Salzmann *et al.*[108] performed a comparative analysis of the thermodynamical properties of metastable ices IV and XII. In particular, the triple point for the metastable equilibria IV – XII – liquid were located at 0.5 – 0.6 GPa and ~267 K in the intersection of melting curves of ices IV (see Ref. 4) and XII (see Ref. 5). Since both ices IV and XII are completely proton-disordered,[6, 90, 103, 104] they should be characterised by a nearly zero entropy difference. Based on the Clapeyron – Clausius equilibrium, this means that the boundary between the phases IV and XII should be nearly parallel to the temperature axis. Ice IV is more stable at $P < 0.5 - 0.6$ GPa, since its melting curve lies above that of ice XII under these conditions.[108] In contrast, ice XII becomes more stable above this threshold pressure. Surprisingly, the temperature-induced transition XII → IV was observed experimentally [90] at 0.6 – 0.7 GPa, *i.e.*, in the region of the higher stability of ice XII according to the above thermodynamic arguments. Salzmann *et al.*[108] noted that the accuracy of the experimental measurement of pressure [90] was of the order of 0.1 GPa, which can explain the apparent discrepancy: likely, the pressure of the transition XII → IV was actually lower than the reported value [90] of 0.6 – 0.7 GPa, *i.e.*, it lied in the region of higher stability of ice IV.

8. Transformations of quenched high-pressure ices upon heating at atmospheric pressure

As was established quite a long time ago, many high-pressure ices recovered at atmospheric pressure in their metastable quenched forms readily transform into ice Ic upon annealing. In particular, annealing of quenched ices II, IX, V and VI at $P = 1$ bar yields metastable ice Ic, which converts into thermodynamically stable ice Ih at higher temperature.[13, 14, 109] The rates of these transitions depend on temperature and thermal prehistory of the sample under study. These processes can be utilised for the production of ice Ic in large quantities.[13]

However, not all quenched high-pressure ices transform into ice Ic upon annealing at atmospheric pressure. For instance, quenched ice VIII first converts into LDA and only then the subsequent transitions LDA → Ic and further Ic → Ih occur.[15] Like in the previous case, the temperature and rate of the transition depend on the heating rate. In particular, at a heating rate of 10 K h^{-1}, the transitions VIII → LDA, LDA → Ic and Ic → Ih are revealed in thermograms as peaks centred at 136 K, 148 K and 210 K, respectively.[15]

Quenched ice VII′ prepared by compression of ice VI first to 3.8 GPa and then to 5.4 GPa at 95 K followed by pressure release to atmospheric pressure at a temperature of 100 K undergoes similar thermal transformations.[12] In this case, a slow temperature increase to 115 K initiates gradual ordering of ice VII′ into ice VIII, then the transformation of ices VII′ and VIII into LDA starts at $T = 125$ K, which is completed after annealing of the sample at 138 K for 1.5 h. The neutron diffraction pattern of the sample heated to 152 K is fully consistent with that of Ic.[12]

There have been several reports [16, 17] that quenched ice VIII converts into LDA and HDA simultaneously upon heating to 130 – 135 K at a rate of 1 K min^{-1}. This conclusion was derived on the basis of neutron diffraction data. In a more recent study,[12] similar neutron diffraction patterns were obtained but the conclusion [16, 17] on the formation of HDA was questioned. Klotz *et al.* [12] argued that the peak observed in the neutron diffraction patterns previously attributed [16, 17] to HDA was too narrow for an amorphous phase and thus its appearance should rather be explained by an admixture of an unidentified crystalline phase. Furthermore, it is known [21] that HDA irreversibly converts into LDA above 125 K. Therefore, we may conclude with a high level of confidence that the temperature-induced conversion of quenched ice VIII into LDA is not accompanied by the concomitant formation of HDA.

In summary, heating of quenched ices VII′ and VIII brings about their transformation into LDA, which in turn converts into Ic and further to Ih. Although both phases VII′ and VIII behave similarly, ice VII′ undergoes partial ordering to ice VIII and the transition VII′ → LDA starts at lower temperature than the respective transition VIII → LDA.

According to the most recent data,[18, 104, 107] quenched ice XII also transforms into ice Ic upon heating at atmospheric pressure. We would like to remind that it is ice XII, which is crystallised within its low-temperature metastability region from HDA during heating, that can be quenched. The conversion of quenched ice XII first prepared at atmospheric pressure by Koza *et al.* [104] into ice Ic upon heating to $T > 135$ K was reported. More recently, the thermal transition of quenched ice XII into ice Ic at $P = 1$ bar was studied in more detail.[18] In this study, samples of ice XII were repeatedly heated to a specific (ever increasing) temperature ranged from 113 K to 183 K, maintained at this temperature for 5 min and cooled down to 93 K to register the X-ray diffraction pattern.[18] The diffraction pattern obtained fully corresponded to the transition XII → Ic revealing no evidence of any amorphous phase.

Based on the high rate of the crystallisation of ice XII from HDA, a close relation between the structures of these two phases was suggested [3] (see Section III.7). With this respect, Tulk and Klug [110] proposed, disregarding the X-ray diffraction results,[18] that quenched ice XII should behave in a way similar to HDA upon heating, *i.e.*, transform first into LDA and only then into ice Ic. They recorded Raman spectra [110] of a sample of ice XII maintained at 12 K, heated to 120 K at a rate of 10 K min^{-1}, maintained at this temperature for several minutes, heated to 130 K at the same rate and maintained at this temperature for 15 min. The spectra registered at 12 and 130 K were ascribed to the crystalline phases XII and Ic, respectively, whereas a broad peak revealed in the spectrum measured at 120 K was attributed [110] to LDA. Thus, based on the Raman spectra they concluded that quenched ice XII indeed behaves analogously to ices VII′ and VIII: upon annealing at atmospheric pressure it transforms first into LDA, which in turn converts further into ice Ic.

Salzmann *et al.*[107] also recorded Raman spectra in ice XII during heating from 80 K to 150 K at a rate of 2 K min^{-1}. They observed that the positions of bands typical of ice XII drifted slightly with an increase in temperature; new bands typical of ice Ic emerged at 140 K, the bands of ice XII disappeared at about 150 K indicating that the transition XII → Ic was complete. No evidence of the intermediate formation of an amorphous phase was observed in agreement with the X-ray diffraction study cited above.[18] Rationalising the discrepancy with the previous Raman study,[110] Salzmann *et al.*[107] speculated that the initial sample in the study by Tulk *et al.*[110] could be some phase other than ice XII. At least, that sample was not attested with diffraction methods, while its reported Raman spectrum[110] differed from that of crystallographically characterised ice XII.[107]

We may thus state with a high level of confidence that ice XII, like ices II, IX, V and VI transforms upon heating at atmospheric pressure directly to ice Ic, which in turn converts into ice Ih with a further increase in temperature. For ice IV, this sequence of transitions was also confirmed[111] using Raman spectroscopy for the temperature range of $80 < T < 145$ K (at a heating rate of 2 K min^{-1}). It is of note that ices Ic and Ih cannot be distinguished by their Raman spectra and thus the formation of Ic was suggested[107,111] only by analogy with the behaviour of other quenched ices.

Summarising all the experimental evidence discussed above, the annealing of quenched high-pressure ices II, IX, V, VI, IV and XII at $P = 1$ bar induces their transformation directly to Ic, whereas ice VII′ and VIII first convert into LDA and only then the subsequent transition LDA → Ic occurs. Ice Ic converts into ice Ih upon further heating. Ice XI is stable at atmospheric pressure, it converts into ice Ih upon heating to 72–74 K.[33,34] Ice III cannot be recovered at atmospheric pressure in the quenched form by the standard cooling at high pressure due to the inevitable transition III → IX. At the same time, no information is available on the thermal transformations at $P = 1$ bar of quenched low-temperature ice III′ prepared[90] by the isobaric heating of HDA at 0.2–0.3 GPa. Ice X has not yet been obtained in the quenched form due to its transition into ice VIII upon pressure release.

IV. Inelastic neutron scattering spectroscopy of water ices

Vibrational spectroscopy can provide valuable information on the potential of the interactions between water molecules in various condensed phases since vibrational frequencies of a molecule are determined by the shape of the corresponding potential well. However, the interpretation of low-frequency part of conventional IR and Raman spectra of water phases is challenging due to the complex pattern of vibrational motions of H-bonded water molecules including acoustic, translational optical and libration modes. The parameters of molecular vibrations can be retrieved in the most straightforward way from inelastic neutron scattering, since INS spectra relate to the density of vibrational states of water molecules in a relatively simple manner.[38,112] The INS spectra of quenched ices Ih, Ic, II, IX, V, VI, VII, VIII and XI, as well as of LDA and HDA (for both H_2O and D_2O) measured at atmospheric pressure at 15 K have been comprehensively analysed.[112]

The INS spectra of ices Ih and Ic are virtually identical.[112] This can be explained by the fact that vibrational spectra of condensed water phases are primarily determined by the interactions of water molecules with their proximate rather than long-range environment and the local environments of H_2O molecules in these two proton-disordered ices are identical: the closest oxygen neighbours reside in the vertices of a nearly ideal tetrahedron at distances of ~2.75–2.76 Å. The INS spectrum of LDA that features a local structure very similar to the structures of Ih and Ic (see Section III.6) also looks similar to those of Ih and Ic.

The INS spectra of ices Ih and Ic reveal two peaks at 28 meV‡ and 37 meV with an integral intensity ratio of ~1 : 2 in the region of translational optical vibrations. These two peaks are located at nearly the same positions for H_2O and D_2O; they are observed in the spectra of both polycrystalline powders and single crystals (irrespective of their orientation).[112] Lattice dynamics and molecular dynamics simulations using traditional interaction potentials for water molecules failed to reproduce these two features in the low-frequency region.[38,112] In 1993, Li and Ross suggested[38] that the split band of translational vibrations can be due to the presence of two types of hydrogen bonds (*viz.*, strong and weak one) in the structures of these ices, which become inequivalent due to different mutual orientations of adjacent molecules (see Fig. 2).

Since only bonding configurations depicted in Figs 2 *c* and 2 *d* are possible in the crystal structure of Ic, the number of former configurations should be twice as that of latter configurations in the case of a random distribution of protons obeying the Bernal–Fowler rules. With this respect, a model for the simulation of vibrational spectra of ices Ic and Ih was developed,[38] which assumed that two types of H-bonds, *viz.*, strong and weak ones, described by different force constants are present in the crystal structures of ices Ih and Ic in a ratio of 2 : 1.

It is of note that the above ratio of strong and weak H-bonds valid for the structure of Ic should be different in the case of ice Ih, since only one third of the hydrogen bonds between the hexagonal layers can adopt the configuration depicted in Fig. 2 *a* from mere geometrical considerations. Nevertheless, the model assumed[38,112] that the structure of Ih also features two strong H-bonds per weak one. A simulation within the lattice dynamics approach for a simulation box composed of eight unit cells of ice Ih with a random distribution of strong and weak bonds (in a ratio of 2 : 1) with the optimised force constants provided good agreement between the theoretical and experimental spectra; in particular, the peaks at 28 and 37 meV were quantitatively reproduced.[38,112] The best-fit values for the force constants were 2.1 and 1.1 eV $Å^{-2}$ for the strong and weak H-bonds, respectively. It is of note that the empirically optimised ratio between the force constants, *i.e.*, 2.1 : 1.1, significantly exceeds the value that can be estimated based on the electrostatic repulsion of protons. In order to explain this discrepancy, the authors of the model[38,112] speculated that the electron density distribution for a specific water molecule is highly sensitive to the orientations of surrounding molecules.

For the crystal structure of proton-ordered ice VIII, this model predicts the presence of only weak H-bonds (see Fig. 2 *b*). The feature corresponding to strong bonds should thus be absent in the vibrational spectra of ice VIII. This fully agrees with the experimental INS spectrum of ice VIII.[112] Furthermore, the spectrum of proton-disordered ice VII should reveal the band of strong H-bonds, which again agrees with the experiment.[112] Meanwhile, the INS spectrum of proton-disordered ice XI (which includes both strong and weak H-bonds in a ratio of 3 : 1) simulated within the model of two force constants appeared drastically different from the experimental spectrum in the region of translational vibrations, which was rather similar to the spectrum of ice Ih.[112,113] Likely, the model of two force constants for the hydrogen bonds represents merely a convenient empirical model, which well reproduces the spectra of ices Ih and Ic, since it was parametrised (as regards the values of force constants and the relative number of strong and weak bonds) just for this case but is not always applicable to the description of spectra of other water ices.

A comparison of INS spectra of ices Ih and XI, on the one hand, and of ices VII and VIII, on the other hand, demonstrates[112] that the spectra of proton-ordered phases reveal distinct narrow peaks, whereas the spectra of related proton-disordered phases are significantly smoother. The same is also true for IR and

‡ 1 meV = 8.066 cm^{-1}.

Raman spectra. This is due to the fact that water molecules in the structures of proton-ordered ices with only one crystallographic type of oxygen atoms have identical environments thus occupying potential wells with identical shapes. Meanwhile, the shapes of potential wells, which depend on both local and long-range environment, in the proton-disordered ices somewhat differ even for identically oriented water molecules with the oxygen atoms of the same crystallographic type. This gives rise to broadening of peaks in the vibrational spectra of proton-disordered ices and their general smoothing as compared to the respective spectra of proton-ordered ices.

The model of two force constants [38, 112] was extended to the case of ice II.[114] The translational region of its INS spectrum was reproduced to a high accuracy within a model that considered water molecules as points. Five force constants were introduced for the description of intermolecular interactions, two of them were selected to be identical and equal to that of the strong H-bond (2.1 eV $Å^{-2}$) from the respective model [38, 112] of ice Ih. The representation of molecules as points becomes insufficient for the calculation of librations, which required introduction of nine force constants. The simulations enabled an assignment of the peaks observed in the low-frequency part of the experimental INS spectrum to specific types of translational vibrations of water molecules in the crystal structure of ice II. A splitting of the libration band to a well-resolved sharp maximum at 68 meV and two broader bands, which resembles the respective region in the spectra of ice Ih, is characteristic of the INS spectrum of ice II.[114]

The lower-frequency boundary of the libration region in the INS spectra shifts towards lower energies in the series Ih – IX – II – V – VI – VIII.[112] This shift reaches the maximum value of about 12 meV for ices VI and VIII. The spectrum of LDA (H_2O) is characterised by a similar shift (13 meV). The INS spectrum of ice VI has other common features with that of HDA (both for H_2O [115] and D_2O [116]), which allowed Kolesnikov *et al.*[115, 116] to suggest that similar dynamical properties of water molecules in HDA and ice VI are due to similar local environments of water molecules in these structures, which gives rise to potential wells with similar shapes. In particular, they proposed [115, 116] that domains of two interpenetrating but not interlinked frameworks of hydrogen bonds observed in the structure of ice VI are also characteristic of HDA. Note that the libration band in the INS spectrum of ice VI, like that of ice II, can be subdivided into three regions, including a well-resolved peak, which is however somewhat broader than the corresponding peak at *ca.* 60 meV in the spectrum of proton-ordered ice II. No similar peak was observed in the libration band of the INS spectrum of HDA.

The shift in the libration band boundary in INS spectra towards lower energies correlates with an elongation of mean O···O distances along the series I – IX – II – V – VI – VIII.[117] This regularity is of common character. For instance, according to pressure-dependent INS spectroscopy of ice II, the lower-frequency boundary of the libration band shifts towards higher frequencies with an increase in pressure, which results in shortening of mean O···O distances.[117] Furthermore, the lower-frequency boundary of the libration band in the INS spectrum of ice II-based helium clathrate hydrate (which is, in overall, quite similar to that of helium-free ice II) is shifted towards lower frequencies in agreement with somewhat elongated mean O···O distances.[46]

An introduction of a small amount of H_2O into D_2O results in the incorporation of HOD molecules into the crystal structure, which violates periodicity. Vibrations of such impurity molecules give rise to narrow localised defect modes at frequencies differing from the vibrations of the whole lattice. Three defect modes characteristic of an HOD molecule can be attributed to different shifts of its H atom within the D_2O lattice. The μ_3 mode corresponds to shifts of the H atom along the hydrogen bond; the μ_2 mode emerges due to vibrations within the HOD plane perpendicular to the hydrogen bond; and the third defect mode, μ_1, corresponds to vibrations in the direction orthogonal to the first two. This type of vibrations of H atoms within HOD molecules was elucidated for quenched D_2O ices Ih, II, VIII and HDA at atmospheric pressure using INS.[118]

The peak corresponding to the low-frequency μ_1 mode shifts towards lower frequencies in the series Ih – II – VIII – HDA. The μ_1 band of ice VIII has a regular Gaussian profile, whereas in the case of ice Ih, it can be well approximated only with two Gaussians, which is in agreement with the model of two force constants. The peak corresponding to the high-frequency μ_3 mode shifts towards higher frequencies along the same series. Meanwhile, there is virtually no difference between frequencies corresponding to the μ_2 mode for various ice phases. It is of note that the shape of the μ_1 band can be also explained without recourse to the model of two force constants.[119]

Therefore, inelastic neutron scattering provides essential information on the vibrational spectrum of water molecules constituting various ice phases, which makes it possible to analyse the character of the intermolecular interactions therein.

V. Computer simulations of crystalline ices

Molecular dynamics (MD) represents yet another powerful tool that makes it possible to evaluate dynamical properties of water molecules in various condensed phases.[120] This is a general method for the numerical simulation of possible states adopted by a many-particle system, which is based on the integration of the Newton equations for all atoms constituting the system under study. The MD method can be applied to water systems only provided that the potentials of interactions between all atoms from both the same and different water molecules are known. Presently, a number of different potentials applicable to the simulation of water systems have been elaborated, however their comprehensive survey lies beyond the scope of the present review. Some advantages and disadvantages of several most common potentials are discussed elsewhere.[121 – 123]

Molecular dynamics can be applied to direct computational problems aimed at the prediction of specific numerical values of desired parameters and to model problems pursuing the exploration of possible qualitative trends in the system behaviour irrespective of exact values. The first type of problems include, for instance, calculations of the equations of states for various ice phases. In this case, the resultant numerical values usually strongly depend on the potential selected. The second type of problems are diverse and numerous; among them, the following can be mentioned: verification of the stability of a real or hypothetical crystalline phase at a given interaction potential, elucidation of the character of motion of separate atoms or the whole molecule, monitoring of structural transitions at the molecular or atomic level, *etc*. In contrast to the first type of problems, specific parameters of the interparticle interactions are often not essential in such simulations, since in the case of a reasonably selected potential, the qualitative simulation results much less depend on its exact parameters. Below we consider some recent works on MD simulation of condensed water phases, including the problems of both types.

Borzsák and Cummings [124] elucidated the structural stability of a hypothetical proton-ordered analogue of ice XII as a function of proton configuration. The model structure had the same oxygen sublattice and unit cell as ice XII. For such a unit cell, ninety different proton configurations conserving the periodicity of the structure are possible with exactly one proton on every hydrogen bond and exactly two protons covalently bound to every oxygen atom.[124] All these possible configurations were simulated using molecular dynamics with the TIP4P potential [23] for a runtime of 100 ps. Only twenty-one configurations proved stable, whereas the remaining structures (both polarised and non-polarised) collapsed during the simulation. The most stable proton configuration in the proton-ordered ice XII analogue corresponded to a structure polarised along the *c* axis.[124] Note that after publication of these computational results, partial proton

ordering in ice XII upon prolonged storage at 110–115 K was suggested based on the experimental DSC data, although the character of this ordering was not clarified [59] (see Section III.7).

Ayala and Tchijov [125] calculated specific volumes v of ices III and V as a function of pressure at a specific temperature (246 K for ice III and 238 K for ice V) and as a function of temperature at a specific pressure (0.25 GPa for ice III and 0.5 GPa for ice V). They used molecular dynamics within the *NPT* ensemble with the TIP4P and TIP5P interaction potentials (see Ref. 126). In this computer experiment, the studied ice phases did not melt at pressures and temperatures lying within their regions of stability. Nevertheless, ice V did melt around the point $T = 268$ K, $P = 0.5$ GPa with the TIP4P potential, whereas the TIP5P showed no melting. For both ice phases, the two potentials afforded differently looking functions $v_T(P)$, *i.e.*, specific volume *vs.* pressure at constant temperature. More specifically, the curve $v_T(P)$ obtained with the TIP5P potential was located lower than that obtained with the TIP4P potential and both curves were lower than the respective curve $v_T(P)$ estimated from the experimental data.[49] As for the function $v_P(T)$, the TIP5P potential again yielded lower values of specific volume for both ice phases considered.

Báez and Clancy [127] calculated various parameters of the transitions liquid–crystal for a number of real and hypothetical ices at atmospheric pressure. The simulation was performed using the non-equilibrium molecular dynamics with the SPC/E potential (see Ref. 128). In contrast to the case of real water, the SPC/E-based simulation predicted that it is ice B,[127] a novel phase with a density higher than that of ice Ih, which was not observed experimentally, rather than ice Ih that should be the most stable crystalline phase at 100 Pa. The authors also attempted to grow various crystalline ices from the melt (*i.e.*, liquid water) at the respective ice–melt interface in the course of the simulation. In the case of ice II–melt interface, they observed a growth of ice II on some parts of the interface and partial melting on other areas in the same computer experiment, thus it was impossible to decisively conclude on the possibility of growth of ice II crystals in the model system. Meanwhile, in the case of the hypothetical ice B–melt interface, stable growth of ice B crystals was clearly observed. Furthermore, the phase B spontaneously formed from another hypothetical ice A (which has the structure of ice IX with a modified proton arrangement) in a simulation of ice A–liquid interface.[127] It is of note however that since the SPC/E potential rather poorly reproduces experimental properties of water and water ices, these results are mainly of methodical significance.

Zheligovskaya *et al.*[129] utilised MD to elucidate the dynamical properties of H_2O molecules in ices II and IX. The interactions between water molecules was described using the Poltev–Malenkov (PM) potential;[130, 131] the simulation was performed within the *NVE* ensemble for two values of the total energy of the system corresponding to temperatures of 82 and 201 K for ice II and of 87 and 203 K for ice IX. According to the direct visual control and a hydrogen bond analysis, the structures of these ices survived the simulation at the temperatures used.

The crystal structures of ices II and IX are proton-ordered and include two crystallographically different H_2O molecules. The following characteristics were calculated for the whole system: the mean-square displacement of the centre of gravity of water molecules as a function of time

$$\langle \boldsymbol{r}^2(t) \rangle = \frac{1}{N} \sum_{i=1}^{N} [\boldsymbol{r}_i(t) - \boldsymbol{r}_i(0)]^2$$

[$\boldsymbol{r}_i(t)$ is the radius-vector to the centre of gravity of the ith molecule at a time moment t; the summation is performed over all N molecules in the system], the autocorrelation function of velocities of centres of gravity of water molecules

$$c(t) = \frac{\frac{1}{N} \sum_{i=1}^{N} [\boldsymbol{v}_i(t) \boldsymbol{v}_i(0)]}{\frac{1}{N} \sum_{i=1}^{N} [\boldsymbol{v}_i(0) \boldsymbol{v}_i(0)]}$$

[$\boldsymbol{v}_i(t)$ is the velocity vector of the gravity centre of the ith water molecule at a time moment t] and the autocorrelation function of velocities of hydrogen atoms $c_H(t)$ (given by a similar formula). These parameters were also calculated separately for each of the two subsystems of crystallographically equivalent water molecules.

Different local environments of crystallographically non-equivalent water molecules lead to the respective difference in their dynamical characteristics. In particular, the amplitude of translational vibrations of the water molecules $H_2O(1)$ constituting corrugated six-membered rings in the crystal structure of ice II appeared somewhat larger than that of the molecules $H_2O(2)$ that constitute flattened rings (see Fig. 3). Similarly, in the case of ice IX, the amplitude of translational vibrations of the water molecules $H_2O(1)$ constituting helices was smaller than that of the water molecules $H_2O(2)$ that link the helices into the united framework (see Fig. 5 *b*). Based on the autocorrelation function of velocities of centres of gravity of water molecules, the density of translational vibrational states was calculated, whereas the density of librational vibrational states was derived from the autocorrelation function of velocities of hydrogen atoms. The derived densities of librational and translational vibrational states were slightly different for crystallographically non-equivalent water molecules for the structures of both ices II and IX. A comparison of the theoretical density of librational vibrational states with the experimental INS spectra indicates [132] that the use of the PM potential underestimates the position of the libration band with respect to that in the experimental spectrum.

As has been mentioned above, in the case of proton-disordered ices, dynamical characteristics differ even for both crystallographically independent molecules and molecules with crystallographically identical O atoms even those possessing O–H bonds with the same orientation. The effects of the proton order on the dynamical characteristics of water molecules in crystalline ices were elucidated with proton-disordered ice III and its proton-ordered counterpart, ice IX, as examples.[133] As in the previous case,[129] ices III and IX were simulated using MD with the PM potential within the *NVE* ensemble. The same parameters as listed above [129] were calculated for all water molecules in the model, separately for the crystallographically non-equivalent molecules $H_2O(1)$ and $H_2O(2)$ and, in the case of ice III, additionally for all water molecules with specifically oriented protons. According to the results obtained, the difference between the dynamical characteristics of the molecules $H_2O(1)$ and $H_2O(2)$ was significantly larger in ice IX than in its proton-disordered analogue, ice III. Furthermore, the theoretical spectrum of librational vibrations of ice III was more smeared as compared to that of ice IX. This is due to the presence of ten different types of orientations of water molecules [six orientation for $H_2O(1)$ and four more orientations for $H_2O(2)$] in ice III instead of only two possible orientations in ice IX. Moreover, both local and long-range environments of water molecules can be different even for identically oriented molecules. Therefore, the spectrum of ice IX formally represents a superposition of two spectra, whereas the spectrum of ice III represents a superposition of a significantly larger number of spectra corresponding to molecules in different environments, which gives rise to its apparent smoothing.

The PM potential was also employed [134] in simulations of proton-disordered metastable ices IV and XII. As in the two studies cited above,[129, 133] the MD simulation was performed within the *NVE* ensemble. The mean temperature was fixed at about 70 K. The structure of ice IV partially collapsed during the simulation, whereas ice XII survived the simulation and preserved its integrity. The self-entangled framework of hydrogen bonds in ice IV contains, as the main structural unit, rings built up of six

water molecules with the oxygen atom O(1) pierced by a 'needle' composed of two H-bonded water molecules with the oxygen atom O(2) (see Fig. 7). The O(2)···O(2) hydrogen bonds in ice IV are elongated to 2.916 Å; each oxygen atom O(2) has short contacts of only 3.14–3.29 Å with six O(1) atoms forming no H-bonds with it.[103] Therefore, the collapse of the structure of ice IV started with the cleavage of the long O(2)···O(2) hydrogen bond followed by the formation of initially absent O(2)···O(1) hydrogen bonds.

The six-membered rings initially present in ice IV were mainly preserved after such a transformation and thus they survived the simulation. The metastable ice XII survived the simulation, which made it possible to calculate dynamical characteristics (the same as discussed above [129, 133] for ices II, IX and III) of the constituent water molecules. As expected, the theoretical parameters of the crystallographically non-equivalent water molecules $H_2O(1)$ and $H_2O(2)$ in the structure of ice XII proved somewhat different.

According to the recent calculations by Henry [135] using the DFT-based method PACHA (Partial Atomic Charges and Hardnesses Analysis), ice IV is indeed characterised by the most strained structure among all known water ices. Based on the computational results obtained, Henry proposed [135] a corrected structural model for ice IV without the elongated O(2)···O(2) hydrogen bonds. (It has to be however stressed that the reported [103] crystal structure of ice IV is correct since it was confirmed in a more recent study.[90]) Difficulties in the experimental preparation of ice IV and its rapid spontaneous conversion into more stable phases at 250 K consistently indicate the relatively low stability of this structure.[4] From this standpoint, its collapse during the computer experiment [134] does not look surprising.

The diffusion of noble-gas atoms and surplus water molecules not incorporated into the crystal structure through the frameworks of crystalline water ices was a subject of several studies. For example, an MD study on the diffusion of water molecules and helium atoms through the crystals of Ih showed [136] that the mechanisms of the diffusion of He atoms and surplus H_2O molecules through the framework of Ih are different in principle. Helium atoms migrate by jumps from one stable position in a cavity of the framework of Ih to another cavity, which makes virtually no effects on vibrations of water molecules forming the framework. In contrast, surplus water molecules not incorporated into the crystalline framework form short-lived hydrogen bonds with the molecules of the framework and thus their diffusion should be accompanied by cleavage and formation of new H-bonds.

Another MD study [137] of dynamical characteristics of Ar and He atoms in the water framework of ice II showed that Ar atoms diffuse in ice II neither along the hexagonal channels, nor through their walls. At the same time, in the case of He atoms filling a part of cavities inside the channels, single jumps of helium atoms to adjacent cavities within the same channel were detected.

Finally, Matsumoto *et al.*[138] reported the first observation of crystallisation of ice from the bulk of liquid water in a molecular dynamics experiment. They simulated a system composed of 512 water molecules within the *NVT* ensemble using the TIP4P potential. The crystallisation process in the system was initiated at a time moment $t = 0$ by an abrupt temperature decrease to 230 K after a prolonged preliminary thermalisation at 400 K.

The process of crystallisation of ice from the bulk of liquid water in this simulation proceeded in four distinct steps. In the first step, there were no stable nuclei of a crystalline phase in the system. This step was characterised by a relatively high and nearly constant potential energy of the system. The fluctuating network of hydrogen bonds involved five-, six- and seven-membered rings in nearly constant proportions. The first step completed at a time moment $t \approx 256$ ns with the spontaneous generation of a local stable polyhedral structure of long-lived hydrogen bonds with strengths above the system average.

In the second step of the crystallisation process, the polyhedral structure was slowly growing up while migrating through the system with gradual decrease in the potential energy. The nucleus of a crystalline phase settled at a certain place to a time moment $t \approx 290$ ns and its rapid growth started, which corresponded to the third crystallisation step. The network of hydrogen bonds within the growing nucleus included predominantly six-membered rings. The energy of the system was rapidly decreasing. At the end of the process, *i.e.*, at the moment of about $t \approx 320$ ns, the nucleus already encompassed the entire volume of the model system. This started the fourth crystallisation step. During this step, the network of hydrogen bonds was gradually approaching the regular structure of ice Ih, which gave only insignificant gain in the potential energy.

Matsumoto *et al.*[138] did not specify the overall duration of the computer experiment (*i.e.*, the CPU runtime expended), but it is evident that the experiment lasted for many months. This fact together with the stochastic nature of the wait time before the generation of a crystalline nucleus make this study unique and difficult to reproduce.

We would like to emphasise that this was the very first MD-based computer experiment [138] that clearly tracked the spontaneous crystallisation from the bulk of liquid at the molecular level. Previously, the crystallisation from a liquid phase was observed in computer experiments only in the presence of a predefined crystalline surface [127] or under external electric field (see Ref. 139).

Computer experiments related to water crystallisation under an external impact or boundary conditions can be illustrated by another example, *viz.*, an MD simulation of the crystallisation of water in a narrow slit between two hydrophobic walls.[140] The model included 960 water molecules confined between two planar hydrophobic walls at a distance adjusted to < 1 nm so as to accommodate two molecular layers. The interactions between water molecules were described with the TIP4P potential, whereas the interactions between water molecules and the walls were described with the 9-3 Lennard-Jones-type potential. The simulation was performed within the *NPT* ensemble According to the simulation, a bilayer amorphous phase was gradually formed from the initial confined liquid water volume upon a decrease in temperature. The layers constituting the amorphous phase were nearly planar and included five-, six- and seven-membered rings. The two layers were related to each other to within a high accuracy by a symmetry plane going in the middle of the gap parallel to the walls. Each water molecule in the bilayer amorphous phase formed four hydrogen bonds (three bonds with the molecules from the same layer and an additional bond with its mirror image from the second layer). Upon further decrease in temperature, this amorphous phase started to crystallise into a bilayer crystalline phase composed of two hexagonal layers arranged one above another and linked by vertical hydrogen bonds. In contrast to the Ih structure comprised of corrugated hexagonal layers with one hydrogen bond to the upper layer and one to the lower layer per a six-membered ring, the resultant bilayer structure [140] consists of nearly flat hexagonal layers with two hydrogen bonds to the bottom layer per a six-membered ring of the upper layer. This result implies that the confinement effects can give rise to the formation of water structures non-typical of bulk phases, *e.g.*, in hydrophobic nanopores.

The formation of unusual structures upon cooling of water incorporated in nanopores even in the case of wettable walls was observed in yet another computer experiment.[141] It is known that carbon nanotubes are wetted with water and thus water can penetrate inside due to the capillary effect. According to the MD simulation [141] of the behaviour of water inside carbon nanotubes with an internal diameter ranged from 1.1 nm to 1.4 nm, water molecules can assemble at sufficiently low temperatures into nanotubes with square, pentagonal, hexagonal or heptagonal cross-sections, depending on the diameter of the carbon nanotube. Note that experimental investigations [10, 11] into the crystallisation

of water within small pores of silicate materials also demonstrated that this process differs from bulk water crystallisation and thus can lead to another outcome.

VI. Occurrence of high-pressure ices in nature

Under terrestrial conditions, the pressure in ice strata never exceeds a few hundred atmospheres and the temperature never goes below 180 K. Therefore, high-pressure ices do not occur on Earth. Typically, frozen water occurs on Earth as hexagonal ice Ih or as a component of gas hydrates, a detailed consideration of which is beyond the scope of the present review.

Ice strata in Antarctica and Greenland have been maintained at low temperature for a long period. Fukazawa *et al.*[142] suggested that this could have resulted in at least partial positional proton ordering, *i.e.*, the transition to proton-ordered ice XI could have started. In order to verify this hypothesis, several ice probes retrieved from depths of 200 m (temperature of 213 K and age of 8000 years) and 350 m (temperature of 214 K and age of 15000 years) of an Antarctica's ice shelf were studied by means of INS.[142] The spectra obtained manifested some features typical of the INS spectra of ice XI, which suggested that the studied samples of ice from the Antarctica's ice shelves have indeed transformed into ice XI.[142] However, the INS spectra of analogous ices retrieved from depths ranged from 200 m (age of 1000 years) to 5500 m (age of more than 10^6 years) of Greenland's ice shelves were fully consistent [143] with the respective spectra of ordinary ice Ih. The authors of the latter study [143] argued that ice samples analysed in the former study [142] also represented ordinary ice Ih and the INS features were misinterpreted due to the insufficient signal-to-noise ratio and low resolution.

Bina and Navrotsky proposed a model [144] of geological processes proceeding upon subduction of the oceanic lithosphere that considered the formation and accumulation of ice VII in large quantities as a possible consequence of the oceanic bed lowering. It is of note however that this is only one of many hypotheses concerning geological processes in the Earth's mantle.

Water ices can also occur in the Earth's atmosphere. Many types of halos around Moon and Sun and other related optical phenomena can be explained by refraction of light upon propagation through crystals of ice Ih suspended in atmosphere. A rare type of such a halo due to the light deflection by 28° have been observed several times, which cannot be explained by the refraction in crystals of ice Ih.[145] This halo can be rationalised under the assumption of emergence of small octahedral crystals of ice Ic in the atmosphere, since light refraction in such crystals can result in the deflection exactly by 27.4° (see Ref. 145). The shape of several types of snow-flakes with ice Ih crystals twinned at 70° is another evidence of the formation of small crystals of ice Ic in the Earth's atmosphere. Such a twinning can be explained by the epitaxy of the (0001) planes of hexagonal ice Ih on the family of symmetry related {111} planes of octahedral crystallites of ice Ic acting as nuclei for the growth of the snow-flake.[146]

Therefore, only occurrence of Ih in the Earth's mantle is reliably established, although there is serious experimental evidence that both ice Ih and Ic can form in the Earth's atmosphere as small crystals.

There are 18 orbs with radii more than 100 km composed to a large extent of water ices within the Solar system.[147] These are the largest Jupiter's satellites, *viz*., Europa, Io, Ganymede and Callisto, Saturn's satellites, *viz*., Mimas, Enceladus, Tethys, Dione, Rhea, Titan, Hyperion and Iapetus, Uranus' satellites, *viz*., Ariel, Umbriel, Titania and Oberon, a Neptune's satellite, Triton, and the Pluto–Charon system. Observations of these orbs were performed from the Earth and, in some cases, from the spacecrafts passing by. Among them, the Jupiter's and Saturn's satellites are the best studied.

The presence of water ices on a surface of an orb can be suggested based on the results of IR photometry or reflectometry. A low mean density of an orb is another indicator of a large water fraction in its interior. The densities of the orbs listed above except for Europa (with $\rho = 3.0$ g cm^{-3}) do not exceed 2 g cm^{-3}, whereas all known rocks have densities more than 2.5 g cm^{-3}.

For the four largest Jupiter's satellites, Ganymede, Europa, Callisto and Io, spherically symmetrical density distributions were simulated to be consistent with the available data on their radii, mean densities and moments of inertia.[148] Based on the densities obtained, the composition of mantle-forming rocks and the

VII. Appendix

Table. Crystallographic parameters of the structures of crystalline ices.

Ice	Space group	T, P [a]	Unit cell parameters	Z [b]	ρ /g cm^{-3}	Degree of proton ordering	Ref.
Ih(H_2O)	$P6_3/mmc$	98 K, 1 bar	a = 4.48 Å, c = 7.31 Å	4	0.92	completely disordered	63
Ic(H_2O)	$Fd\bar{3}m$	98 K, 1 bar	a = 6.350 Å	8	0.92	the same	63
II(H_2O)	$R\bar{3}$	123 K, 1 bar	a = 7.78 Å, α = 113.1°	12	1.17	completely ordered	44
III(D_2O)	$P4_12_12$	240 K, 0.25 GPa	a = 6.67 Å, c = 6.96 Å	12	1.286	disordered	54
IV(D_2O)	$R\bar{3}c$	110 K, 1 bar	a = 7.60 Å, α = 70.1°	16	1.272	completely disordered	103
V(H_2O)	$A2/a$	98 K, 1 bar	a = 9.22 Å, b = 7.54 Å, c = 10.35 Å, β = 109.2°	28	1.231	disordered	57
V(D_2O)	$A2/a$	234 K, 0.5 GPa	a = 9.0926 Å, b = 7.5409 Å, c = 10.2547 Å, β = 109.14°	28	1.400	the same	54
VI(H_2O)	$P4_2/nmc$	98 K, 1 bar	a = 6.27 Å, c = 5.79 Å	10	1.31	completely disordered	63
VI(D_2O)	$P4_2/nmc$	225 K, 1.1 GPa	a = 6.1812 Å, c = 5.6980 Å	10	1.526	the same	60
VII(D_2O)	$Pn\bar{3}m$	295 K, 2.4 GPa	a = 3.344 Å	2	1.778	"	60
VIII(D_2O)	$I4_1/amd$	10 K, 2.4 GPa	a = 4.656 Å, c = 6.775 Å	8	1.810	completely ordered	60
IX(D_2O)	$P4_12_12$	110 K, 1 bar	a = 6.73 Å, c = 6.83 Å	12	1.13	ordered	55
X(H_2O, D_2O)	$Pn\bar{3}m$	–	–	2	–	the protons reside in the middle of the O···O bonds	
XI(D_2O)	$Cmc2_1$	5 K, 1 bar	a = 4.502 Å, b = 7.798 Å, c = 7.328 Å	8	0.93	ordered	28
XII(D_2O)	$I\bar{4}2d$	260 K, 0.50 GPa	a = 8.304 Å, c = 4.024 Å	12	1.4365	disordered	6
XII(D_2O)	$I\bar{4}2d$	1.5 K, 1 bar	a = 8.2816 Å, c = 4.0361 Å	12	1.4397	the same	104

[a] Temperature and pressure at which the structure was determined; [b] the number of water molecules (the number of formula units for ice X) per unit cell.

possible thicknesses of the outer crusts from water ices were estimated. For Ganymede and Callisto, the models were further refined according to the data on the surface heat radiation, presumed intensity of heat generation in their cores due to the radioactive decay, heat conductivity of mantle components and of the outer ice crust to predict the depth distributions of densities, temperatures and pressures. Based on these data altogether, the occurrence of high-pressure ices therein was concluded. The results of measurements of the magnetic fields around the satellites were also utilised, which can support either the presence or absence of an iron core creating an own magnetic field around the satellite or the presence of an internal conductive ocean from liquid water with dissolved salts, which affects the magnetic field induced by Jupiter.

The following conclusions were derived based on these calculations.[148] Io is composed of a core (mostly from Fe and FeS) with a radius of 38% to 53% of its total radius (1821.6 km) surrounded by an outer shell of olivine rocks. No water is present in Io. The radius of the central core of Europa (composed of pure or FeS-contaminated iron) amounts 10% to 45% of the total radius of this satellite (1565 km), its mantle is composed of olivine rocks, the outermost shell represents a crust from water ices with a thickness from 120 to 170 km. Ganymede has a core with a radius of 1/4 to 1/3 of its total radius (2634 km), the mantle is also dominantly composed of olivine rocks, whereas its outer ice crust with a thickness of 900 km is subdivided into concentric shells of ices VI, V, III and I. Water ices and rocks are probably at least partly spatially separated also in Callisto (with a radius of 2410.3 km); among ice forms, ices VI, V, III and I can occur there.

As for the investigated Saturn's satellites, the density of Titan is 1.9 g cm^{-3}, densities of other satellites range from 1.4 g cm^{-3} to 1.0 g cm^{-3}. This strongly suggests that the composition of all the investigated Saturn's satellites but Titan is dominated by water ices. According to simulations of the structure of Titan's interior, the Titan's core is either composed of only silicate rocks or represents a core–shell structure with a central core from molten iron and an outer shell of silicate rocks.[149] The core is surrounded by a mantle composed of several layers, including ice VI, other high-pressure ices and clathrate hydrates, then liquid water and the outermost layer of ice Ih.[149]

Therefore, there is serious evidence that crystalline high-pressure ices indeed occur in some satellites of larger planets in the Solar system.

* * *

Solid water phases have remained in the focus of interest of researchers over the last 15 years. A new crystalline modification, ice XII, has been discovered; transitions between crystalline ices, amorphisation of crystalline ices and crystallisation of amorphous ices have been elucidated in detail. The data obtained clearly demonstrate that water polymorphism is truly multi-faceted and no other substance can compete with water in the diversity of forms. We believe that the nearest future will witness more striking investigations into water, especially, its non-equilibrium forms and transitions between them.

The present review has been written with a partial financial support of the Russian Foundation for Basic Research (Project No. 03-03-32227).

References

1. P V Hobbs *Ice Physics* (Oxford: Clarendon Press, 1974)
2. E Whalley, J B R Heath, D W Davidson *J. Chem. Phys.* **48** 2362 (1968)
3. T Loerting, I Kohl, C Salzmann, E Mayer, A Hallbrucker *J. Chem. Phys.* **116** 3171 (2002)
4. H Engelhardt, E Whalley *J. Chem. Phys.* **56** 2678 (1972)
5. I-M Chou, J G Blank, A F Goncharov, H Mao, R J Hemley *Science* **281** 809 (1998)
6. C Lobban, J L Finney, W F Kuhs *Nature (London)* **391** 268 (1998)
7. L Pauling *J. Am. Chem. Soc.* **57** 2680 (1935)
8. E F Burton, W F Oliver *Proc. R. Soc. London, Ser. A* **153** 166 (1936)
9. I Kohl, E Mayer, A Hallbrucker *Phys. Chem. Chem. Phys.* **2** 1579 (2000)
10. M-C Bellissent-Funel, in *New Kinds of Phase Transitions: Transformations in Disordered Substances. NATO Science Series. II. Mathematics, Physics and Chemistry* Vol. 81 (Eds V V Brazhkin, S V Buldyrev, V N Ryzhov, H E Stanley) (Dordrecht: Kluwer Academic, 2002) p. 335
11. J Dore, B Webber, P Behrens, C Haggenmuller, D Montague, in *New Kinds of Phase Transitions: Transformations in Disordered Substances. NATO Science Series. II. Mathematics, Physics and Chemistry* Vol. 81 (Eds V V Brazhkin, S V Buldyrev, V N Ryzhov, H E Stanley) (Dordrecht: Kluwer Academic, 2002) p. 469
12. S Klotz, J M Besson, G Hamel, R J Nelmes, J S Loveday, W G Marshall *Nature (London)* **398** 681 (1999)
13. J E Bertie, L D Calvert, E Whalley *J. Chem. Phys.* **38** 840 (1963)
14. J E Bertie, L D Calvert, E Whalley *Can. J. Chem.* **42** 1373 (1964)
15. D D Klug, Y P Handa, J S Tse, E Whalley *J. Chem. Phys.* **90** 2390 (1989)
16. A M Balagurov, O I Barkalov, A I Kolesnikov, G M Mironova, E G Ponyatovskii, V V Sinitsin, V K Fedotov *Pis'ma Zh. Eksp. Teor. Fiz.* **53** 30 (1991) [a]
17. A I Kolesnikov, V V Sinitsyn, E G Ponyatovsky, I Natkaniec, L S Smirnov, J-C Li *J. Phys. Chem. B* **101** 6082 (1997)
18. I Kohl, E Mayer, A Hallbrucker *J. Phys. Chem. B* **104** 12102 (2000)
19. G P Johari, A Hallbrucker, E Mayer *Nature (London)* **330** 552 (1987)
20. O Mishima, L D Calvert, E Whalley *Nature (London)* **310** 393 (1984)
21. O Mishima, L D Calvert, E Whalley *Nature (London)* **314** 76 (1985)
22. K Röttger, A Endriss, J Ihringer, S Doyle, W F Kuhs *Acta Crystallogr., Sect. B* **50** 644 (1994)
23. W L Jorgensen, J Chandrasekhar, J D Madura, R W Impey, M L Klein *J. Chem. Phys.* **79** 926 (1983)
24. H Tanaka *J. Chem. Phys.* **108** 4887 (1998)
25. H Tanaka *J. Mol. Struct. (THEOCHEM)* **461–462** 561 (1999)
26. V Carravetta, E Clementi *J. Chem. Phys.* **81** 2646 (1984)
27. T Matsuo, Y Tajima, H Suga *J. Phys. Chem. Solids* **47** 165 (1986)
28. A J Leadbetter, R C Ward, J W Clark, P A Tucker, T Matsuo, H Suga *J. Chem. Phys.* **82** 424 (1985)
29. R Howe, R W Whitworth *J. Chem. Phys.* **90** 4450 (1989)
30. E R Davidson, K Morokuma *J. Chem. Phys.* **81** 3741 (1984)
31. G T Barkema, J de Boer *J. Chem. Phys.* **99** 2059 (1993)
32. J Lekner *Physica B* **252** 149 (1998)
33. S M Jackson, R W Whitworth *J. Chem. Phys.* **103** 7647 (1995)
34. S M Jackson, R W Whitworth *J. Phys. Chem. B* **101** 6177 (1997)
35. C M B Line, R W Whitworth *J. Chem. Phys.* **104** 10008 (1996)
36. S M Jackson, V M Nield, R W Whitworth, M Oguro, C C Wilson *J. Phys. Chem. B* **101** 6142 (1997)
37. H Fukazawa, S Ikeda, M Oguro, T Fukumura, S Mae *J. Phys. Chem. B* **106** 6021 (2002)
38. J-C Li, D K Ross *Nature (London)* **365** 327 (1993)
39. M V Kirov *Zh. Strukt. Khim.* **37** 1089 (1996) [b]
40. M V Kirov *Zh. Strukt. Khim.* **42** 701 (2001) [b]
41. M V Kirov *Zh. Strukt. Khim.* **42** 712 (2001) [b]
42. M J Iedema, M J Dresser, D L Doering, J B Rowland, W P Hess, A A Tsekouras, J P Cowin *J. Phys. Chem. B* **102** 9203 (1998)
43. X Su, L Lianos, Y R Shen, G A Somorjai *Phys. Rev. Lett.* **80** 1533 (1998)
44. B Kamb *Acta Crystallogr.* **17** 1437 (1964)
45. A Yu Manakov, Yu A Dyadin *Ros. Khim. Zh.* **47** (3) 28 (2003) [c]
46. G G Malenkov, I Natkaniec, L S Smirnov, L Bobrowicz-Sarga, S I Bragin *High Pressure Res.* **16** 201 (1999)

47. D Londono, J L Finney, W F Kuhs *J. Chem. Phys.* **97** 547 (1992)
48. C Lobban, J L Finney, W F Kuhs *J. Chem. Phys.* **117** 3928 (2002)
49. R E Gagnon, H Kiefte, M J Clouter, E Whalley *J. Chem. Phys.* **92** 1909 (1990)
50. A D Fortes, I G Wood, J P Brodholt, L Vocadlo *J. Chem. Phys.* **119** 4567 (2003)
51. G G Malenkov, Doctoral Thesis in Chemical Sciences, Institute of Physical Chemistry, Academy of Sciences of the USSR, Moscow, 1990
52. Y Wang, J C Li *Can. J. Phys.* **81** 409 (2003)
53. J D Londono, W F Kuhs, J L Finney *J. Chem. Phys.* **98** 4878 (1993)
54. C Lobban, J L Finney, W F Kuhs *J. Chem. Phys.* **112** 7169 (2000)
55. S J La Placa, W C Hamilton, B Kamb, A Prakash *J. Chem. Phys.* **58** 567 (1973)
56. K Nishibata, E Whalley *J. Chem. Phys.* **60** 3189 (1974)
57. B Kamb, A Prakash, C Knobler *Acta Crystallogr.* **22** 706 (1967)
58. G P Johari, E Whalley *J. Chem. Phys.* **115** 3274 (2001)
59. C G Salzmann, I Kohl, T Loerting, E Mayer, A Hallbrucker *Phys. Chem. Chem. Phys.* **5** 3507 (2003)
60. W F Kuhs, J L Finney, C Vettier, D V Bliss *J. Chem. Phys.* **81** 3612 (1984)
61. J D Jorgensen, T G Worlton *J. Chem. Phys.* **83** 329 (1985)
62. J D Jorgensen, R A Beyerlein, N Watanabe, T G Worlton *J. Chem. Phys.* **81** 3211 (1984)
63. B Kamb *Science* **150** 205 (1965)
64. E Whalley, D W Davidson, J B R Heath *J. Chem. Phys.* **45** 3976 (1966)
65. R J Nelmes, J S Loveday, W G Marshall, G Hamel, J M Besson, S Klotz *Phys. Rev. Lett.* **81** 2719 (1998)
66. R J Nelmes, J S Loveday, R M Wilson, J M Besson, Ph Pruzan, S Klotz, G Hamel, S Hull *Phys. Rev. Lett.* **71** 1192 (1993)
67. J M Besson, Ph Pruzan, S Klotz, G Hamel, B Silvi, R J Nelmes, J S Loveday, R M Wilson, S Hull *Phys. Rev. B* **49** 12540 (1994)
68. J M Besson, S Klotz, G Hamel, W G Marshall, R J Nelmes, J S Loveday *Phys. Rev. Lett.* **78** 3141 (1997)
69. M Kobayashi, T Nanba, M Kamada, S Endo *J. Phys.: Condens. Matter* **10** 11551 (1998)
70. R J Hemley, L C Chen, H K Mao *Nature (London)* **338** 638 (1989)
71. M Song, H Yamawaki, H Fujihisa, M Sakashita, K Aoki *Phys. Rev. B* **68** 024108 (2003)
72. W B Holzapfel, *J. Chem. Phys.* **56** 712 (1972)
73. K S Schweizer, F H Stillinger *J. Chem. Phys.* **80** 1230 (1984)
74. M Benoit, D Marx, M Parrinello *Nature (London)* **392** 258 (1998)
75. J Teixeira *Nature (London)* **392** 232 (1998)
76. M Benoit, A H Romero, D Marx *Phys. Rev. Lett.* **89** 145501 (2002)
77. R J Hemley, A P Jephcoat, H K Mao, C S Zha, L W Finger, D E Cox *Nature (London)* **330** 737 (1987)
78. P Loubeyre, R LeToullec, E Wolanin, M Hanfland, D Hausermann *Nature (London)* **397** 503 (1999)
79. K Aoki, H Yamawaki, M Sakashita, H Fujihisa *Phys. Rev. B* **54** 15673 (1996)
80. A F Goncharov, V V Struzhkin, M S Somayazulu, R J Hemley, H K Mao *Science* **273** 218 (1996)
81. P Pruzan, J C Chervin, B Canny *J. Chem. Phys.* **99** 9842 (1993)
82. A F Goncharov, V V Struzhkin, H K Mao, R J Hemley *Phys. Rev. Lett.* **83** 1998 (1999)
83. M Song, H Yamawaki, H Fujihisa, M Sakashita, K Aoki *Phys. Rev. B* **68** 014106 (2003)
84. B Schwager, L Chudinovskikh, A Gavriliuk, R Boehler *J. Phys.: Condens. Matter* **16** S1177 (2004)
85. E Katoh, H Yamawaki, H Fujihisa, M Sakashita, K Aoki *Science* **295** 1264 (2002)
86. A H Narten, C G Venkatesh, S A Rice *J. Chem. Phys.* **64** 1106 (1976)
87. P G Debenedetti *J. Phys.: Condens. Matter* **15** R1669 (2003)
88. G P Johari *J. Phys. Chem.* **94** 1212 (1990)
89. O Mishima *J. Chem. Phys.* **100** 5910 (1994)
90. S Klotz, G Hamel, J S Loveday, R J Nelmes, M Guthrie *Z. Kristallogr.* **218** 117 (2003)
91. C G Salzmann, T Loerting, I Kohl, E Mayer, A Hallbrucker *J. Phys. Chem. B* **106** 5587 (2002)
92. T Loerting, C Salzmann, I Kohl, E Mayer, A Hallbrucker *Phys. Chem. Chem. Phys.* **3** 5355 (2001)
93. S Klotz, G Hamel, J S Loveday, R J Nelmes, M Guthrie, A K Soper *Phys. Rev. Lett.* **89** 285502 (2002)
94. O Mishima, H E Stanley *Nature (London)* **396** 329 (1998)
95. G P Johari *Phys. Chem. Chem. Phys.* **2** 1567 (2000)
96. E G Ponyatovsky, V V Sinitsyn *Physica B* **265** 121 (1999)
97. E G Ponyatovski *J. Phys.: Condens. Matter* **15** 6123 (2003)
98. E L Gromnitskaya, O V Stal'gorova, V V Brazhkin, A G Lyapin *Phys. Rev. B* **64** 094205 (2001)
99. A G Lyapin, O V Stal'gorova, E L Gromnitskaya, V V Brazhkin *Zh. Eksp. Teor. Fiz.* **121** 335 (2002) [d]
100. V V Brazhkin, A G Lyapin *J. Phys.: Condens. Matter* **15** 6059 (2003)
101. P W Bridgman *Proc. Am. Acad. Arts Sci.* **47** 441 (1912)
102. P W Bridgman *J. Chem. Phys.* **3** 597 (1935)
103. H Engelhardt, B Kamb *J. Chem. Phys.* **75** 5887 (1981)
104. M M Koza, H Schober, T Hansen, A Tölle, F Fujara *Phys. Rev. Lett.* **84** 4112 (2000)
105. I Kohl, E Mayer, A Hallbrucker *Phys. Chem. Chem. Phys.* **3** 602 (2001)
106. G P Johari *J. Chem. Phys.* **118** 242 (2003)
107. C Salzmann, I Kohl, T Loerting, E Mayer, A Hallbrucker *J. Phys. Chem. B* **106** 1 (2002)
108. C G Salzmann, E Mayer, A Hallbrucker *Phys. Chem. Chem. Phys.* **6** 1269 (2004)
109. Y P Handa, D D Klug, E Whalley *Can. J. Chem.* **66** 919 (1988)
110. C A Tulk, D D Klug *Phys. Rev. B* **63** 212201 (2001)
111. C G Salzmann, I Kohl, T Loerting, E Mayer, A Hallbrucker *J. Phys. Chem. B* **107** 2802 (2003)
112. J Li *J. Chem. Phys.* **105** 6733 (1996)
113. H Fukazawa, S Ikeda, S Mae *Chem. Phys. Lett.* **282** 215 (1998)
114. S L Dong, Y Wang, A I Kolesnikov, J C Li *J. Chem. Phys.* **109** 235 (1998)
115. A I Kolesnikov, V V Sinitsyn, E G Ponyatovsky, I Natkaniec, L S Smirnov *J. Phys.: Condens. Matter* **6** 375 (1994)
116. A I Kolesnikov, J C Li, N C Ahmad, C-K Loong, J Nipko, D Yocum, S F Parker *Physica B* **263–264** 650 (1999)
117. L S Smirnov, A N Ivanov, A I Kolesnikov, I Natkaniec *High Pressure Res.* **16** 187 (1999)
118. J C Li, Y Wang, S L Dong, P Zhang, A I Kolesnikov *J. Chem. Phys.* **119** 3332 (2003)
119. J S Tse, D D Klug *Phys. Lett. A* **198** 464 (1995)
120. Yu K Tovbin (Ed.) *Metod Molekulyarnoi Dinamiki v Fizicheskoi Khimii* (Method of Molecular Dynamic in Physical Chemistry) (Moscow: Nauka, 1996)
121. V E Petrenko, M L Dubova, Yu M Kessler, M Yu Perova *Zh. Fiz. Khim.* **74** 1957 (2000) [e]
122. V E Petrenko, Yu M Kessler, M L Antipova, A Yu Nikiforov, N A Abakumova *Zh. Fiz. Khim.* **76** 271 (2002) [e]
123. Yu M Kessler, V E Petrenko, M L Antipova, A V Borovkov *Zh. Fiz. Khim.* **76** 1924 (2002) [e]
124. I Borzsàk, P T Cummings *Chem. Phys. Lett.* **300** 359 (1999)
125. R B Ayala, V Tchijov *Can. J. Phys.* **81** 11 (2003)
126. M W Mahoney, W L Jorgensen *J. Chem. Phys.* **112** 8910 (2000)
127. L A Báez, P Clancy *J. Chem. Phys.* **103** 9744 (1995)
128. H J C Berendsen, J R Grigera, T P Straatsma *J. Phys. Chem.* **91** 6269 (1987)
129. E A Zheligovskaya, G G Malenkov, A A Averkiev *Zh. Strukt. Khim.* **42** 10 (2001) [b]
130. V I Poltev, T I Grokhlina, G G Malenkov *J. Biomol. Struct. Dyn.* **2** 413 (1984)
131. V I Poltev, G G Malenkov, E J Gonzalez, A V Teplukhin, R Rein, M Shibata, J H Miller *J. Biomol. Struct. Dyn.* **13** 717 (1996)
132. G G Malenkov, E A Zheligovskaya, A A Averkiev, I Natkaniec, L S Smirnov, L Bobrovicz-Sarga, S I Bragin *High Pressure Res.* **17** 273 (2000)
133. E A Zheligovskaya *Zh. Strukt. Khim.* **44** 897 (2003) [b]
134. E A Zheligovskaya, G G Malenkov *Zh. Strukt. Khim.* **46** 284 (2005) [b]
135. M Henry *ChemPhysChem* **3** 607 (2002)

136. T Ikeda-Fukazawa, S Horikawa, T Hondoh, K Kawamura *J. Chem. Phys.* **117** 3886 (2002)
137. G G Malenkov, E A Zheligovskaya *J. Inclusion Phenom. Macrocycl. Chem.* **48** 45 (2004)
138. M Matsumoto, S Saito, I Ohmine *Nature (London)* **416** 409 (2002)
139. I M Svishchev, P G Kusalik *Phys. Rev. Lett.* **73** 975 (1994)
140. K Koga, H Tanaka, X C Zeng *Nature (London)* **408** 564 (2000)
141. K Koga, G T Gao, H Tanaka, X C Zeng *Nature (London)* **412** 802 (2001)
142. H Fukazawa, S Mae, S Ikeda, O Watanabe *Chem. Phys. Lett.* **294** 554 (1998)
143. Y Wang, J C Li, A I Kolesnikov, S Parker, S J Johnsen *Physica B* **276** 282 (2000)
144. C R Bina, A Navrotsky *Nature (London)* **408** 844 (2000)
145. E Whalley *J. Phys. Chem.* **87** 4174 (1983)
146. T Kobayashi, Y Furukawa, T Takahashi *J. Cryst. Growth* **35** 262 (1976)
147. G J Consolmagno *J. Phys. Chem.* **87** 4204 (1983)
148. F Sohl, T Spohn, D Breuer, K Nagel *Icarus* **157** 104 (2002)
149. O Grasset, C Sotin, F Deschamps *Planet. Space Sci.* **48** 617 (2000)

[a] — *J. Exp. Theor. Phys. Lett. (Engl. Transl.)*
[b] — *J. Struct. Chem. (Engl. Transl.)*
[c] — *Mendeleev Chem. J. (Engl. Transl.)*
[d] — *J. Exp. Theor. Phys. (Engl. Transl.)*
[e] — *Russ. J. Phys. Chem. (Engl. Transl.)*